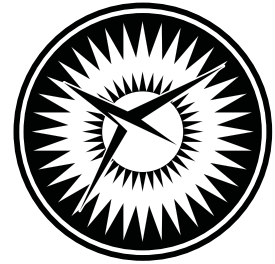


NASA/CR-2010-216723
NIA Report No. 2010-04



NATIONAL
INSTITUTE OF
AEROSPACE



Development of a Benchmark Example for Delamination Fatigue Growth Prediction

Ronald Krueger
National Institute of Aerospace, Hampton, Virginia

July 2010

NASA STI Program . . . in Profile

Since its founding, NASA has been dedicated to the advancement of aeronautics and space science. The NASA scientific and technical information (STI) program plays a key part in helping NASA maintain this important role.

The NASA STI program operates under the auspices of the Agency Chief Information Officer. It collects, organizes, provides for archiving, and disseminates NASA's STI. The NASA STI program provides access to the NASA Aeronautics and Space Database and its public interface, the NASA Technical Report Server, thus providing one of the largest collections of aeronautical and space science STI in the world. Results are published in both non-NASA channels and by NASA in the NASA STI Report Series, which includes the following report types:

- **TECHNICAL PUBLICATION.** Reports of completed research or a major significant phase of research that present the results of NASA programs and include extensive data or theoretical analysis. Includes compilations of significant scientific and technical data and information deemed to be of continuing reference value. NASA counterpart of peer-reviewed formal professional papers, but having less stringent limitations on manuscript length and extent of graphic presentations.
- **TECHNICAL MEMORANDUM.** Scientific and technical findings that are preliminary or of specialized interest, e.g., quick release reports, working papers, and bibliographies that contain minimal annotation. Does not contain extensive analysis.
- **CONTRACTOR REPORT.** Scientific and technical findings by NASA-sponsored contractors and grantees.

- **CONFERENCE PUBLICATION.** Collected papers from scientific and technical conferences, symposia, seminars, or other meetings sponsored or co-sponsored by NASA.
- **SPECIAL PUBLICATION.** Scientific, technical, or historical information from NASA programs, projects, and missions, often concerned with subjects having substantial public interest.
- **TECHNICAL TRANSLATION.** English-language translations of foreign scientific and technical material pertinent to NASA's mission.

Specialized services also include creating custom thesauri, building customized databases, and organizing and publishing research results.

For more information about the NASA STI program, see the following:

- Access the NASA STI program home page at <http://www.sti.nasa.gov>
- E-mail your question via the Internet to help@sti.nasa.gov
- Fax your question to the NASA STI Help Desk at 443-757-5803
- Phone the NASA STI Help Desk at 443-757-5802
- Write to:
NASA STI Help Desk
NASA Center for AeroSpace Information
7115 Standard Drive
Hanover, MD 21076-1320

NASA/CR-2010-216723
NIA Report No. 2010-04



Development of a Benchmark Example for Delamination Fatigue Growth Prediction

Ronald Krueger
National Institute of Aerospace, Hampton, Virginia

National Aeronautics and
Space Administration

Langley Research Center
Hampton, Virginia 23681-2199

Prepared for Langley Research Center
under Contract NNL09AA00A

July 2010

Trade names and trademarks are used in this report for identification only. Their usage does not constitute an official endorsement, either expressed or implied, by the National Aeronautics and Space Administration.

Available from:

NASA Center for AeroSpace Information
7115 Standard Drive
Hanover, MD 21076-1320
443-757-5802

DEVELOPMENT OF A BENCHMARK EXAMPLE FOR DELAMINATION FATIGUE GROWTH PREDICTION

Ronald Krueger*

ABSTRACT

The development of a benchmark example for cyclic delamination growth prediction is presented and demonstrated for a commercial code. The example is based on a finite element model of a Double Cantilever Beam (DCB) specimen, which is independent of the analysis software used and allows the assessment of the delamination growth prediction capabilities in commercial finite element codes. First, the benchmark result was created for the specimen: The number of cycles to delamination onset was calculated from the material data for mode I fatigue delamination growth onset. Then, the number of cycles during stable delamination growth was obtained incrementally from the material data for mode I fatigue delamination propagation. For the benchmark case, where the results for delamination onset and growth were combined, the delamination length was calculated for an increasing total number of load cycles. Second, starting from an initially straight front, the delamination was allowed to grow under cyclic loading in a finite element model of a commercial code. The number of cycles to delamination onset and the number of cycles during stable delamination growth for each growth increment were obtained from the analysis. In general, good agreement between the results obtained from the growth analysis and the benchmark results could be achieved by selecting the appropriate input parameters. Overall, the results are encouraging but further assessment for mixed-mode delamination is required.

1. INTRODUCTION

Over the past two decades, the use of fracture mechanics has become common practice to characterize the onset and growth of delaminations. In order to predict delamination onset or growth, the calculated strain energy release rate components are compared to interlaminar fracture toughness properties measured over a range from pure mode I loading to pure mode II loading.

The virtual crack closure technique (VCCT) is widely used for computing energy release rates based on results from continuum (2D) and solid (3D) finite element (FE) analyses and to supply the mode separation required when using the mixed-mode fracture criterion [1, 2]. The virtual crack closure technique was recently implemented into several commercial finite element codes. As new methods for analyzing composite delamination are incorporated into finite element codes, the need for comparison and benchmarking becomes important since each code requires specific input parameters unique to its implementation.

An approach for assessing the delamination propagation capabilities in commercial finite element codes under static loading was recently presented and demonstrated for VCCT for ABAQUS[®] [3, 4]. In these recent papers, benchmark results were created for full three-dimensional finite element models of the Double Cantilever Beam (DCB) and the Single Leg Bending (SLB) specimen. Then, starting from an initially straight front, the delamination was allowed to propagate in the finite element model. The load-displacement relationship and the total strain energy obtained from the propagation analysis results and the benchmark results were compared and good

*R. Krueger, National Institute of Aerospace, 100 Exploration Way, Hampton, VA, 23666, resident at Durability, Damage Tolerance and Reliability Branch, MS 188E, NASA Langley Research Center, Hampton, VA, 23681, USA.

¹ ABAQUS[®] is a product of Dassault Systèmes Simulia Corp. (DSS), Providence, RI, USA

agreements could be achieved by selecting the appropriate input parameters. Overall, the results were encouraging but it was determined that further assessment for mixed-mode delamination is required [3, 4].

The objective of the present study was to create a benchmark example, independent of the analysis software used, which allows the assessment of the delamination fatigue growth prediction capabilities in commercial finite element codes. At the beginning, a benchmark example is created based on incremental finite element models of a DCB specimen. To avoid unnecessary complications, experimental anomalies such as fiber bridging were not addressed. First, a sample material and cyclic loading was selected. Second, the number of cycles to delamination onset, N_D , was calculated from the mode I fatigue delamination growth onset data of the material. Third, the number of cycles during stable delamination growth, ΔN_G , was obtained incrementally from the material data for mode I fatigue delamination propagation by using growth increments of $\Delta a=0.1$ mm. Fourth, the total number of growth cycles, N_G , was calculated by summing over the increments ΔN_G . Fifth, the corresponding delamination length, a , was calculated by summing over the growth increments Δa . Finally, for the benchmark case where results for delamination onset and growth were combined, the delamination length, a , was calculated and plotted versus an increasing total number of load cycles $N_T=N_D+N_G$. After creating the benchmark, the approach was demonstrated for the commercial finite element code ABAQUS[®]. Starting from an initially straight front, the delamination was allowed to grow based on the algorithms implemented into the commercial finite element software. Input control parameters were varied to study the effect on the computed delamination increase during cyclic loading. It was assumed that delamination length increase during cyclic loading obtained from finite element analysis should closely match the growth shown in the benchmark example. The benchmark enabled the selection of the appropriate input parameters that yielded good agreement between the results obtained from the growth analysis and the benchmark results. Once the parameters have been identified, they may then be used with confidence to model delamination growth for more complex configurations.

2. METHODOLOGY

The methodology for delamination propagation, onset and growth was applied to the DCB specimen to create the benchmark example [5, 6]. Since the required material property input data were not readily available in the open literature for a single material, a fictitious set of properties was constructed for this benchmarking exercise. Individual properties for commonly used graphite/epoxy tape materials were obtained from the open literature to create this set to represent a typical graphite epoxy composite. The material properties are given in Tables I and II.

2.1 Static fracture toughness

The mode I fracture toughness (mixed-mode ratio $G_{II}/G_I=0$) is generated experimentally using the Double Cantilever Beam (DCB) tests (as shown in Figure 1) [7]. A fracture toughness $G_{Ic}=0.17$ kJ/m² was used in this benchmarking exercise [8].

2.2 Fatigue delamination growth onset

The number of cycles to delamination onset, N_D , can be obtained from the delamination onset curve plotted in Figure 2 [9, 10]. The onset curve (solid green line) is a power law fit

$$G = m_0 \cdot N_D^{m_1} \quad (1)$$

of the experimental data (open, green circles) obtained from a DCB test using the respective standard for delamination growth onset [9].

2.3 Fatigue delamination growth

The number of cycles during stable delamination growth, N_G , can be obtained from the fatigue delamination propagation relationship (Paris Law) plotted in Figure 3 [8]. The delamination growth rate (solid purple line) can be expressed as a power law function

$$\frac{da}{dN} = c \cdot G_{\max}^n \quad (2)$$

where da/dN is the increase in delamination length per cycle and G_{\max} is the maximum energy release rate at the front at peak loading. The factor c and exponent n are obtained by fitting the curve to the experimental data (open black circles) obtained from DCB tests [8]. The critical energy release rate or fracture toughness, G_{Ic} , was included in the plot of Figure 3 (blue solid vertical line). Since composites do not exhibit the same threshold behavior commonly observed in metals, a cutoff value, G_{th} , was chosen below which delamination growth was assumed to stop (green solid vertical line) [8]. It has to be noted that this benchmarking exercise ignores branching or fiber bridging and hence the Paris Law was not normalized with the static R-curve as recently suggested [11, 12].

3. SPECIMEN AND FATIGUE TEST DESCRIPTION

For the current numerical investigation, the Double Cantilever Beam (DCB) specimen, as shown in Figure 1, was chosen since it is simple, only exhibits the mode I opening fracture mode and had been used previously to develop an approach to assess the quasi-static delamination propagation simulation capabilities in commercial finite element codes [3, 4]. To avoid unnecessary complications, experimental anomalies such as fiber bridging were not addressed. For the current study, a DCB specimen made of graphite/epoxy with an unidirectional layup, $[0]_{24}$, was modeled. The material properties are given in Table I [8]. The material, layup, overall specimen dimensions including initial crack length, a , were identical to the specimen used earlier [3, 4].

For the cyclic loading of the specimen, guidance was taken from a draft standard designed to determine mode I fatigue delamination propagation [11]. In the draft document, it is recommended to start the test at a maximum displacement, δ_{\max} , which causes the energy release rate at the front, $G_{I\max}$, to reach initially about 80% of G_{Ic}

$$\frac{G_{I\max}}{G_{Ic}} = 0.8 \quad (3)$$

The maximum load, P_{\max} , and maximum displacement, $\delta_{\max}/2$, were calculated using the known quadratic relationship between energy release rate and applied load or displacement

$$\frac{G_{I\max}}{G_{Ic}} = \frac{P_{\max}^2}{P_{crit}^2} \Rightarrow P_{\max} = P_{crit} \sqrt{\frac{G_{I\max}}{G_{Ic}}}, \quad \delta_{\max} = \delta_{crit} \sqrt{\frac{G_{I\max}}{G_{Ic}}} \quad (4)$$

$$\delta_{max} = \delta_{crit} \sqrt{0.8} \quad (5)$$

where P_{crit} and δ_{crit} are the critical values. For the current study, a critical energy release rate $G_{Ic}=0.17$ kJ/m² was used and the critical values P_{crit} and δ_{crit} (grey dashed lines) were obtained from the benchmark for static delamination propagation [3, 4] shown in the load-displacement plot in Figure 4. The calculated maximum load, P_{max} , and calculated maximum displacement, $\delta_{max}/2$, are shown in Figure 4 (dashed red line) in relationship to the static benchmark case (solid grey circles and dashed grey line) mentioned above. During constant amplitude cyclic loading of a DCB specimen under displacement control, the applied maximum displacement, $\delta_{max}/2=0.67$ mm, is kept constant while the load drops as the delamination length increases (solid red circles and solid red line). The energy release rate corresponding to an applied maximum displacement $\delta_{max}/2=0.67$ mm was calculated for different delamination lengths a using equation (5). The energy release rate decreases with increasing delamination length, a , as shown in Figure 5 (solid red circles and solid red line). Delamination growth was assumed to stop once the calculated energy release rate drops below the cutoff value, G_{th} , (green solid horizontal line). The static benchmark case (solid grey circles and dashed grey line in Figure 5), where the delamination propagates at constant G_{Ic} (solid blue line in Figure 5) was included for comparison.

In the ASTM draft document, it is suggested to use a load ratio $R=0.1$ for testing [11]. The corresponding minimum load, P_{min} , and minimum displacement, $\delta_{min}/2$, were calculated

$$R = \frac{P_{min}}{P_{max}} = \frac{\delta_{min}}{\delta_{max}} = 0.1 \Rightarrow \delta_{min} = 0.1 \cdot \delta_{max} \quad (6)$$

Further, it was suggested in the ASTM draft document to use a frequency $f=10$ Hz for testing [11]. A graphical representation of the cyclic fatigue loading is plotted in Figure 6. The applied displacement $\delta/2$ is represented as a function of time, t

$$\delta/2 = [a_0 + b_1 \cdot \sin \omega(t - t_0)] \cdot \delta_{max}/2 \quad (7)$$

where $\delta_{max}/2=0.67$ mm is the maximum displacement. The constants $a_0=0.55$, $b_1=0.45$, the circular frequency $\omega=20\pi=62.832$ and the starting time $t_0=0.025$ are calculated from load ratio $R=0.1$ and the frequency $f=10$ Hz for testing. The resulting equation to calculate the applied displacement $\delta/2$ is shown in Figure 6.

4. CREATING A BENCHMARK EXAMPLE FOR GROWTH PREDICTION

4.1 Fatigue delamination growth onset

The number of cycles to delamination onset, N_D , may be obtained by solving equation (1) for N_D .

$$G = m_0 \cdot N_D^{m_1} \Rightarrow N_D = \underbrace{\left(\frac{1}{m_0}\right)^{\frac{1}{m_1}}}_{c_1} \cdot G^{\frac{1}{m_1}} \Rightarrow N_D = c_1 \cdot G^{c_2} \quad (8)$$

where $c_2 = \frac{1}{m_1}$. Values for the constants c_1 and c_2 are shown in Figure 7.

At the beginning of the test, the specimen is loaded initially so that the energy release rate at the front, $G_{I_{max}}$, reaches about 80% of G_{Ic} corresponding to $G_{I_{max}}=0.1362 \text{ kJ/m}^2$. The initial energy release rate is shown in the delamination onset plot of Figure 7 as a horizontal dashed red line. From the delamination onset curve, the number of cycles to delamination onset is determined as, $N_D=150$ shown as a vertical dashed red line.

4.2 Fatigue delamination growth

The number of cycles during stable delamination growth can be obtained by solving equation (2) for N_G

$$N_G = \int dN = \int \frac{1}{c} G_{max}^{-n} \cdot da \quad (9)$$

As mentioned above, the specimen is loaded initially so that the energy release rate at the front, $G_{I_{max}}$, reaches about 80% of G_{Ic} corresponding to $G_{I_{max}}=0.1362 \text{ kJ/m}^2$ in the current study as shown in the Paris Law plot of Figure 8 (solid red square).

For practical applications, equation (2) can be replaced by an incremental equivalent expression

$$\frac{\Delta a}{\Delta N} = c \cdot G_{max}^n \quad (10)$$

where for the current study, increments of $\Delta a=0.1 \text{ mm}$ were chosen. Starting at the initial delamination length $a_0=30.5 \text{ mm}$, the energy release rates $G_{i,max}$ were obtained for each increment, i , from the curve fit (solid red circles and solid red line) plotted in Figure 5. These energy release rate values were then used to obtain the increase in delamination length per cycle or growth rate $\Delta a/\Delta N$ from the Paris Law in Figure 8. The growth rate rapidly decreases with increasing delamination length a as shown in Figure 9 (solid red circles and solid red line). The number of cycles during stable delamination growth, N_G , was calculated by summing the increments ΔN_i

$$N_G = \sum_{i=1}^k \Delta N_i = \sum_{i=1}^k \frac{1}{c} G_{i,max}^{-n} \cdot \Delta a \quad (11)$$

where k is the number of increments. The corresponding delamination length, a , was calculated by adding the incremental lengths Δa to the initial length a_0 .

$$a = a_0 + \sum_{i=1}^k \Delta a = a_0 + k \cdot \Delta a \quad (12)$$

For stable delamination growth, the delamination length, a , is plotted in Figure 10 for an increasing number of load cycles N_G (crosses and solid red line).

4.3 Combined fatigue delamination onset and growth

For the combined case of delamination onset and growth, the total life, N_T , may be expressed as

$$N_T = N_D + N_G \quad (13)$$

where, N_D , is the number of cycles to delamination onset and N_G , is the number of cycles during delamination growth [12]. For this combined case, the delamination length, a , is plotted in Figure 11 for an increasing number of load cycles N_T . For the first N_D cycles, the delamination length remains constant (horizontal red line), followed by a growth section where - over N_G cycles - the delamination length increases following the Paris Law (crosses and solid red line). Once a delamination length is reached where the energy release rate drops below the assumed cutoff value, G_{th} , (as shown in Figure 5) the delamination growth no longer follows the Paris Law (dashed grey line) and stops (horizontal solid red line).

Applying the relationship

$$t = \frac{N}{f}, \quad (14)$$

where t is the time and f is the frequency, the development of the delamination length a can be plotted on a time scale assuming a frequency of 10 Hz as shown in Figure 12 (solid red line).

4.4 Using the benchmark example to assess an automated analysis in a commercial FE code

The load/displacement behavior of the DCB specimen - as shown in Figure 4 (solid red line) - can serve as an initial check for the finite element model. The correct input of model dimensions, material, layup and load application can thus be verified. During initial loading, the load and displacement should increase in a linear fashion and follow the initial slope until the maximum load, P_{max} , and maximum displacement, δ_{max} , are reached. To minimize problems with numerical stability of the analysis, it is suggested that prescribed displacements, $\delta_{max}/2$ and $\delta_{min}/2$ are applied in the analysis instead of nodal point loads, P_{max} and P_{min} . The same approach was used to create the static benchmark case mentioned above [3, 4]. Once the delamination starts to grow, the load is expected to drop while the applied maximum displacement $\delta_{max}/2=0.67$ is expected to remain constant.

The energy release rate may serve as an additional verification step before the delamination growth analysis is initiated. The computed values at the initial crack tip in a 2D model or along the delamination front in a 3D model should reach but not exceed the target value of $G_{I_{max}}=0.136$ kJ/m². Once delamination growth starts in the model, the computed energy release rate should decrease with increasing delamination length, a , as shown in Figure 5. The curve fit (solid red line) can therefore be used to check the computed energy release rate during delamination growth.

The growth rate $\Delta a/\Delta N$, shown in Figure 9, decreases and the curve fit (solid red line) may be used as a check for the correct implementation of the Paris Law provided this output is available. For the delamination growth analysis, the delamination length, a , should increase with the number of cycles, N , as shown in Figure 10. The curve fit (solid red line) can therefore be used as a benchmark.

A delamination length prediction analysis that accounts for delamination fatigue onset as well as stable growth should yield results that closely resemble the plot in Figure 11. The curve fit (solid red line) can therefore be used as a benchmark.

5. FINITE ELEMENT MODELING

A typical two-dimensional finite element model of a Double Cantilever Beam (DCB) specimen is shown in Figure 13. The specimen was modeled with solid plane strain elements (CPE4) and solid plane stress elements (CPS4) in ABAQUS[®] Standard 6.8, 6.9 and 6.9EF. Along the length, all models were divided into different sections with different mesh refinement. The DCB specimen was modeled with six elements through the specimen thickness ($2h$) as shown in the detail of Figure 13b. The resulting element length at the delamination tip was $\Delta a=0.5$ mm. A finer mesh, resulting in $\Delta a=0.25$ mm, was also generated as is shown in Figure 13c. Additionally, three coarser meshes with a reduced number of elements in the length direction were also generated as shown in Figures 14, resulting in $\Delta a=1.0$ mm (Figure 14b), $\Delta a=1.25$ mm (Figure 14c) and $\Delta a=1.67$ mm (Figure 14a).

The plane of delamination was modeled as a discrete discontinuity in the center of the specimen. For the analysis with ABAQUS[®] 6.8, 6.9 and 6.9EF, the models were created as separate meshes for the upper and lower part of the specimens with identical nodal point coordinates in the plane of delamination [13]. Two surfaces (top and bottom surface) were defined to identify the contact area in the plane of delamination as shown in Figure 13b. Additionally, a node set was created to define the intact (bonded nodes) region.

Typical three-dimensional finite element models of the DCB specimen are shown in Figures 15 and 16. Along the length, all models were divided into different sections with different mesh refinement. A refined mesh was used in the center of the DCB specimen as shown in the detail of Figure 15b. Across the width, a uniform mesh was used to avoid potential problems at the transition between a coarse and finer mesh [3,4]. Through the specimen thickness ($2h$), six elements were used as shown in the detail of Figure 15b. The resulting element length at the delamination tip was $\Delta a=0.5$ mm. The specimen was modeled with solid brick elements (C3D8I) which had yielded excellent results in a previous studies [3,4]. Two coarser meshes with a reduced number of elements in the width and length directions, resulting in $\Delta a=1.0$ mm and $\Delta a=2.0$ mm, were also generated as shown in Figures 16a and b.

Three models of the DCB specimen were generated with continuum shell elements (SC8R) as shown in Figures 17a to c. The continuum shell elements in ABAQUS[®] are used to model an entire three-dimensional body. Unlike conventional shells, which model a reference surface, the SC8R elements have displacement degrees of freedom only, use linear interpolation, and allow finite membrane deformation and large rotations and, therefore, are suitable for geometric nonlinear analysis. The continuum shell elements are based on first-order layer-wise composite theory and include the effects of transverse shear deformation and thickness change [13]. In the x - y plane, the models had the same fidelity as the models made of solid brick elements C3D8I shown in Figures 4b, 5a and 5b, resulting in an element length at the delamination tip $\Delta a=0.5$ mm, $\Delta a=1.0$ mm and $\Delta a=2.0$ mm, respectively. In the z -direction, only one element was used to model the thickness of the specimen. These less-refined models were used to study the effect on performance (CPU time), computed load/displacement behavior and growth prediction in comparison with the more refined models discussed above.

For all the analyses performed, the low-cycle fatigue analysis in ABAQUS[®] Standard 6.8, 6.9 and 6.9EF was used to model delamination growth at the interfaces in laminated composites [13, 14]. A direct cyclic approach is part of the implementation and provides a computationally effective modeling technique to obtain the stabilized response of a structure subjected to constant amplitude cyclic loading. The theory and algorithm to obtain a stabilized response using the direct cyclic approach are described in detail in reference 14. Delamination onset and growth predictions are based on the calculation of the strain energy release rate at the delamination front using VCCT. To

determine propagation, computed energy release rates are compared to the input data for onset and growth from experiments as discussed in the methodology section. During the analysis, at least one element length at the crack tip is released along the interface after each stabilized cycle.

For all analyses, the elastic constants, the input to define the fracture criterion, and the parameters for delamination onset and delamination growth (Paris Law) were kept constant. The elastic constants are given in Table I. The fracture toughness values and the parameters required for delamination onset and growth are given in Table II. The parameters to define the load frequency ($f=10$ Hz), the load ratio ($R=0.1$) as well as the minimum and maximum applied displacement ($\delta_{min}/2=0.067$ mm and $\delta_{max}/2=0.67$ mm) were also kept constant during all analyses. To study the effect on the computed onset and growth behavior during the analysis:

- The number of terms used to define a Fourier series was varied. A Fourier series is used during the execution of the ABAQUS[®] Standard to approximate the periodic cyclic loading.
- The size of the initial time increment used in the analysis was varied.
- The input required to define the cyclic loading was altered.
- The release tolerance was varied. Once a user specified release tolerance ($(G - G_c)/G_c > \text{release tolerance}$) is exceeded during the analysis in ABAQUS[®] Standard, a cutback operation is performed which reduces the time increment. The cutback reduces the degree of overshoot and improves the accuracy of the local solution.
- The solution controls were varied.

It was assumed that the computed onset and growth behavior should closely match the benchmark results established earlier. Setting the value of the input parameters correctly is often an iterative procedure, which will be discussed later. Further details about the required input parameters are discussed in the appendix where sample input files are also provided.

6. ANALYSIS

6.1 Static analysis to verify correct input data and model response

First, static analyses were performed with propagation disabled to ensure that the input was correct and that the models responded as expected. For this static analysis, the applied displacement at the tip of the arms was ramped up to the maximum displacement $\delta_{max}/2=0.67$ for all models. To ensure that the model geometry and material input data for all models produced consistent results, the computed load-displacement behavior as shown in Figures 18 and 19 was evaluated. In comparison to the fatigue benchmark (solid grey circles and solid grey line) from Figure 4, which is based on analyses using solid 3D volume elements (C3D8I), the results are in good agreement. The model where plane strain elements (CPE4) were used exhibits a slightly more compliant behavior (dashed blue line) as shown in Figure 18. The model where plane stress elements (CPS4) were used exhibits a slightly stiffer behavior (dash-dot green line) whereas the results from the solid model (C3D8I) are as expected identical (solid black line) to the benchmark results. The results obtained from solid models with different mesh densities (see Figures 15 and 16) and from the continuum shell models (see Figure 17) are in good agreement with the benchmark as shown in Figure 19. Based on the results it was assumed that the geometry, maximum applied displacements and material input were defined correctly and all models adequately represented the benchmark case.

In a second analysis step, only a single load cycle was analyzed, starting at the previously applied maximum displacement $\delta_{max}/2=0.67$. This step was performed to check that the amplitude input was defined correctly and resulted in the desired periodic cyclic loading during the analysis. Therefore, the displacement, $\delta/2$, - obtained as analysis output - was plotted versus the step time, t , as shown in Figure 20. The models where plane strain elements (CPE4) were used (blue crosses) yielded the same output as the models where plane stress elements (CPS4) were used (green x's) and solid model (C3D8I) were used (open black circles). Based on a comparison with the desired fatigue loading (grey line) it is assumed that the amplitude input was defined correctly and the increments are small enough to adequately represent the desired periodic fatigue loading shown in Figure 6.

Additionally, the computed mode I energy release rate – also obtained as analysis output - was plotted versus the step time, t , as shown in Figure 21. As desired, the energy release rate cycles between the expected maximum value $G_{Imax}=0.136 \text{ kJ/m}^2$ and minimum value $G_{Imin}=0.00136 \text{ kJ/m}^2$. The model where plane strain elements (CPE4) were used yields lower energy release rates (blue crosses and solid blue line) while the model where plane stress elements (CPS4) were used yields higher energy release rates (green x's and solid green line) which is consistent with the observations made above with respect to the slight variation in model stiffness. The results from the solid model (C3D8I), taken in the center of the specimen at $y=0.0$, are as expected identical to the benchmark results (open black circles and solid black line).

For the models made of 3D continuum elements (C3D8I and SC8R), the computed mode I strain energy release rate values were also computed for an applied maximum displacement $\delta_{max}/2=0.67$ and plotted versus the normalized width, y/B , of the specimen as shown in Figure 22. The results were obtained from models shown in Figures 15 through 17. Qualitatively, the mode I strain energy release rate is fairly constant in the center part of the specimen and drops progressively towards the edges. As desired, the energy release rate in the center of specimen reached the expected maximum value $G_{Imax}=0.136 \text{ kJ/m}^2$ for all models used. Additionally, these results served as a verification that the VCCT procedure implemented in ABAQUS® 6.8 yielded the same results (open symbols) as an external post-processing routine (crosses) [4]. As expected, the mode II and mode III strain energy release rates were computed to be nearly zero and hence are not shown. Based on results, it was assumed that with respect to the computed energy release rates all models adequately represented the benchmark case.

6.2 Results from fatigue onset and growth analysis

In Figures 23 to 32, the delamination length, a , is plotted versus the number of cycles, N , for different input parameters and models. For all results shown, the analysis stopped when a 10,000,000 cycles limit - used as input to terminate the analysis - was reached.

6.2.1 Initial results

Initial results, as plotted in Figures 23 and 24, were obtained using the specified default values as input parameters (see appendix). The results obtained from two-dimensional plane strain (open blue circles and solid blue line) and plane stress (open red squares and solid red line) models as well as full three-dimensional models (open green diamonds and solid green line) were within 4% of the benchmark results (grey crosses and solid grey line) as shown in Figure 23. For better visualization of the results and to be able to identify the differences in the results, the scale on the vertical axis was expanded as shown in Figure 24. For all results shown, the predicted onset occurs prior to the benchmark result onset, $N_D=150$ cycles. The onset value is lowest for the plane stress results,

followed by the results obtained from 3D solid models and the plane strain results. This sequence can be explained by the computed energy release rate shown in Figure 21, where the values obtained from the plane stress model are slightly higher compared to the results obtained from 3D solid and plane strain models. During the growth phase of the analysis, the results lie on curves with nearly the same slope parallel to the benchmark which suggests that the Paris Law was implemented correctly and is - as expected - independent of the model. For all models, the threshold cutoff, where delamination growth is terminated and the delamination length remains constant, is predicted close to the number of cycles defined by the benchmark.

6.2.2 Variation of input parameters

Input parameters were varied to study the effect on the computed onset and growth behavior during the analysis and results are plotted in Figures 25 to 27. For this parametric study, only models with a refined mesh ($\Delta a=0.25$ mm, see Figure 13c) made of plane strain elements (CPE4) were used. Once a set of parameters was established that yielded good results, the effects of mesh size and element type on the results were studied.

First, the effect of the initial time increment used in the analysis settings was studied as shown in Figure 25 (see appendix for details). The initial time increment was varied between $i_0=0.01$ (one tenth of a single loading cycle, $t_s=0.1$ s, open blue circles and solid blue line) and $i_0=0.0001$ (one thousandth of a single loading cycle, open green diamonds and solid green line). For larger initial time increments, the onset of delamination shifted towards a lower number of cycles. Reducing the initial time increments, however, significantly increased the computation time. Based on the results, it was therefore decided to use an initial time increment of $i_0=0.001$ (open red squares and solid red line) for the remainder of the study to save computation time. This step is justified by the fact that the results obtained for $i_0=0.001$ were almost identical to the values obtained from the analysis where a smaller initial time increment was used ($i_0=0.0001$).

Second, the input to define the cyclic loading was varied. In order to define the cyclic applied displacement, $\delta/2$, a set of parameters need to be determined as shown in the equation in Figures 26 and 27 (see appendix for details). Selecting $A_I=0$ results in a sine curve representation of the cyclic load (analysis results are shown in Figure 26). Selecting $B_I=0$ results in a cosine curve representation of the cyclic load (analysis results are shown in Figure 27). The selection of the starting time, t_0 , causes a phase-shift. Further details about the input parameters are discussed in detail in the appendix where the corresponding cyclic applied displacements $\delta/2$ are plotted in Figure A8. As shown in Figures 26 and 27, the number of cycles to delamination onset is the most sensitive to input variations. The results obtained for the growth phase however, lie on curves with nearly the same slope, parallel to the benchmark. Also the threshold cutoff, where delamination growth is expected to stop and the delamination length remains constant, is predicted close to the number of cycles defined by the benchmark. A narrow band of results (green solid lines), was obtained when the number of terms used to define the Fourier series was increased to 50. A Fourier series is used in ABAQUS[®] Standard during the analysis to approximate the periodic cyclic loading (see appendix). The narrow band of results was in good agreement with the benchmark curve (grey solid line) compared to the results obtained for the default setting of 11 Fourier terms which showed more scatter (black dashed lines). It should be noted that one term in a Fourier series is sufficient to exactly represent a simple periodic function such as the simple sine function used in the current example. At the same time, a large number of terms should improve the approximation of a more complicated cyclic load as demonstrated. It should also be noted that good results could only be obtained when the analyses were performed with ABAQUS[®] Standard 6.9EF.

Earlier versions showed unexplainable wide variations in results. Based on the current results, it was decided to use a sine curve representation ($A_I=0$) in combination with the starting time, $t_0=0.0$ for the remainder of the study.

Third, the release tolerance was varied. Once a user specified release tolerance ($(G - G_c)/G_c > \text{release tolerance}$) is exceeded during the analysis in ABAQUS[®] Standard, a cutback operation is performed which reduces the time increment. The cutback reduces the degree of overshoot and improves the accuracy of the local solution [13]. In the current study, varying the input between 0.2 (the default value) and 0.01 did not have any effect on the computed onset and growth behavior during the analysis. It is assumed that the release tolerance only affects static delamination propagation and not growth under cyclic loading studied here.

Fourth, the solution controls were varied. It is generally not required nor recommended to modify the solution controls in ABAQUS[®] Standard. Since some of the solution controls, however, were modified in the DCB example problem provided by ABAQUS[®] [15], it was decided to briefly address the effect on the computed onset and growth behavior during the analysis. The first input parameter that defines the iteration number at which the periodicity condition is first imposed, was not modified and the default value was kept. A series of analyses were performed where the other four input parameters were varied between 100 and 10^{-4} . Changing the input did not have any effect on the computed onset and growth behavior during the analysis, however it significantly influenced the computation time. The analysis required only about a tenth of the computation time when the second input parameter was modified from the default value ($5 \cdot 10^{-3}$) to values larger than 10^{-1} . Changing the other remaining three parameters did not have any effect for this example. Further details about the input parameters are discussed in the appendix where also sample input files are provided.

6.2.3 Variation of mesh size and element type

The results obtained for models with different mesh sizes and different element types are shown in Figures 28 to 33. For models made of plane strain elements (CPE4), the element length, Δa , at the delamination tip was varied as shown in Figures 13 and 14. The results obtained from the respective models are plotted in Figures 28 and 29. Excellent agreement with the benchmark curve (grey crosses and grey solid line) could be achieved for element lengths up to $\Delta a=1.25$ mm, as shown in Figure 28. For element length $\Delta a=1.67$ mm (purple triangles and solid purple line), the predicted onset occurs for a slightly higher number of cycles. The observed mismatch is largely due to the increased element length, which causes the first growth step to be larger. The following growth increments are relatively large due to the increased element length ($\Delta a=1.67$ mm). However, during the growth phase of the analysis, the results from all models lie on curves with the same slope parallel to the benchmark, which suggests that the Paris Law was implemented correctly and is, as expected independent, of the mesh. The analyses were repeated with the goal to eliminate the onset part of the analysis and focus on the stable growth section. Input parameters were chosen so that the onset part was extremely short and stable growth basically started immediately. Further details about the input parameters are discussed in detail in the appendix. The results are shown in Figure 29. As mentioned above, excellent agreement with the benchmark curve (grey crosses and grey solid line) could be achieved for all element lengths except for element length $\Delta a=1.67$ mm (purple triangles and solid purple line). For all models, the threshold cutoff, where delamination growth is expected to stop and the delamination length remains constant, is predicted close to the

number of cycles defined by the benchmark. The total computation time was between 70 s for the coarsest mesh and 1030 s for the finest mesh as shown in Figure 30¹.

The analyses were repeated for models made of plane stress elements (CPS4), where the element length, Δa , at the delamination tip was varied as before. The results obtained from the respective models are plotted in Figure 31. As before for the plane strain models, excellent agreement with the benchmark curve (grey crosses and grey solid line) could be achieved for all element lengths except for element length $\Delta a=1.67$ mm (purple triangles and solid purple line). The total computation time took between 80 s for the coarsest mesh and 1050 s for the finest mesh¹. The computation times are included in Figure 30 for comparison.

The results obtained for models made of 3D solid and continuum shell elements (shown in Figures 15 to 17) are shown in Figure 32. Good agreement with the benchmark curve (grey crosses and grey solid line) could be achieved for small element lengths ($\Delta a=0.5$ mm). For larger element lengths, the results started to deviate from the benchmark. However, during the growth phase of the analysis, the results from all models lie on curves with the same slope parallel to the benchmark as observed before. Results obtained from the continuum shell element models (blue dashed lines) were almost identical when compared to results obtained from corresponding full 3D solid models (green solid line) with the same element length, Δa . The computational effort, however, was reduced by a factor of 2.5 to 2.9 for analyses performed using the continuum shell element models. For the models made of 3D solid elements, the total computation time was between 5800 s for the coarsest mesh and about 7 days for the finest mesh. For the corresponding models made of continuum shell elements, the total computation time was between 2000 s for the coarsest mesh and about 2.8 days for the finest mesh¹. The computation times are also included in Figure 30 for comparison.

For final comparison, finite element analyses were repeated with two-dimensional and three-dimensional models with the same element length, $\Delta a=0.5$ mm, at the delamination tip. The results obtained from two-dimensional plane strain (open blue circles and solid blue line) and plane stress (open red squares and solid red line) models as well as full 3D solid models (open green diamonds and solid green line) and continuum shell elements (orange x's and solid orange line) were within 1% of the benchmark curve (grey crosses and solid grey line) as shown in Figure 33. The results obtained from the continuum shell element model (orange x's and solid orange line) were almost identical compared to results obtained from the full 3D solid model (open green diamonds and solid green line) as mentioned above. The results obtained from plane stress models (open red squares and solid red line) are close to the results obtained from three-dimensional models. For all results shown, the predicted onset occurs first for the plane stress results and last for the plane strain results. Also, the delamination length obtained from plane strain models are slightly lower. This observation can be explained by looking at the computed energy release rate in Figure 21. The plane stress model yields a slightly higher energy release rate compared to the 3D solid and the plane strain model. Delamination onset would therefore occur first in plane stress models as indicated by the results plotted in Figure 33. During the stable growth phase, however, the results for all models lie on curves with nearly the same slope parallel to the benchmark as mentioned earlier. For all models, the threshold cutoff, where delamination growth is assumed to stop and the delamination length remains constant, is predicted close to the number of cycles defined by the benchmark.

¹ CPU time on Dual-Core AMD Opteron(tm) Processor 8220 SE

7. SUMMARY AND CONCLUSIONS

The development of a benchmark example for cyclic delamination growth prediction is presented and demonstrated for the commercial finite element code ABAQUS[®] Standard. The example is based on a finite element model of a Double Cantilever Beam (DCB) specimen, which is independent of the analysis software used and allows the assessment of the delamination growth prediction capabilities in commercial finite element codes. First, the development of a benchmark example for delamination fatigue growth prediction was presented step by step. The number of cycles to delamination onset was calculated from the material data for mode I fatigue delamination growth onset. The number of cycles during stable delamination growth was obtained incrementally from the material data for mode I fatigue delamination propagation. For the combined benchmark case of delamination onset and growth, the delamination length was calculated for an increasing total number of load cycles. Second, starting from an initially straight front, the delamination was allowed to grow under cyclic loading. The number of cycles to delamination onset and the number of cycles during stable delamination growth for each growth increment were obtained from the analysis.

The results showed the following:

- In general, good agreement between the results obtained from the growth analysis and the benchmark results could be achieved by selecting the appropriate input parameters. However, selecting the appropriate input parameters was not straightforward and often required an iterative procedure.
- The onset prediction appeared much more sensitive to the input parameters than the growth prediction.
- Consistent results were obtained when input parameters were selected such that 50 terms in the Fourier series were used during the execution of ABAQUS[®] Standard to approximate the periodic cyclic loading.
- Good agreement between analysis results and the benchmark could be achieved when the initial time increment used in the analysis was about one tenth of a single loading cycle.
- Best results were obtained when a sine curve representation of the cyclic applied displacement was selected in combination with the starting time, $t_0=0.0$.
- The release tolerance did not have an effect on the analysis or the computed results.
- Accurately computing the onset and growth required fine meshes with an element length at the tip $\Delta a \leq 1.0$ mm.
- The solution controls in ABAQUS[®] Standard had to be modified in order to reduce computation time. Even with carefully selected input parameters, the analyses for three-dimensional models of a simple DCB specimen required days.
- Although implemented in ABAQUS[®] Standard 6.8, version 6.9EF was required to obtain consistently good results.
- Improvements are needed to make this analysis applicable to real case scenarios such as more complex specimens or structural components.

Overall, the results are promising. In a real case scenario, however, where the results are unknown, obtaining the right solution will remain challenging. Further studies are required which should include the assessment of the propagation capabilities in more complex mixed-mode specimens and on a structural level.

Assessing the implementation in one particular finite element code illustrated the value of establishing benchmark solutions since each code requires specific input parameters unique to its implementation. Once the parameters have been identified, they may then be used with confidence to model delamination growth for more complex configurations.

ACKNOWLEDGEMENTS

This research was supported by the Aircraft Aging and Durability Project as part of NASA's Aviation Safety Program.

The analyses were performed at the Durability, Damage Tolerance and Reliability Branch at NASA Langley Research Center, Hampton, Virginia, USA.

The author would like to thank Satish Gadhi of SIMULIA Headquarters and Babu Aminjekarai and Brian Baillargeon of the SIMULIA Eastern Region office for their support and advice in getting this analysis started.

REFERENCES

1. E. F. Rybicki and M. F. Kanninen, "A Finite Element Calculation of Stress Intensity Factors by a Modified Crack Closure Integral," *Eng. Fracture Mech.*, vol. 9, pp. 931-938, 1977.
2. R. Krueger, "Virtual Crack Closure Technique: History, Approach and Applications," *Applied Mechanics Reviews*, vol. 57, pp. 109-143, 2004.
3. R. Krueger, "An Approach for Assessing Delamination Propagation Capabilities in Commercial Finite Element Codes," in proceeding of the *22nd Annual Technical Conference of the American Society for Composites*, Seattle, Washington, 2007.
4. R. Krueger, "An Approach to Assess Delamination Propagation Simulation Capabilities in Commercial Finite Element Codes," NASA/TM-2008-215123, 2008.
5. I. S. Raju and T. K. O'Brien, "Fracture mechanics concepts, stress fields, strain energy release rates, delamination and growth criteria," in *Delamination behavior of composites*, S. Sridharan, Ed.: Woodhead Publishing in Materials, 2008.
6. "Composite Fatigue Damage Onset," in *Composite Materials Handbook CMH-17*. Vol. 3, section 12.6.4, draft of revision G, 2009.
7. "ASTM D 5528-01, Standard Test Method for Mode I Interlaminar Fracture Toughness of Unidirectional Fiber-Reinforced Polymer Matrix Composites," in *Annual Book of ASTM Standards*. vol. 15.03: American Society for Testing and Materials, 2008.
8. M. König, R. Krüger, K. Kussmaul, M. v. Alberti, and M. Gädke, "Characterizing Static and Fatigue Interlaminar Fracture Behaviour of a First Generation Graphite/Epoxy Composite," in *Composite Materials: Testing and Design - (13th Vol.)*, ASTM STP 1242, S. J. Hooper, Ed.: American Society for Testing and Materials, pp. 60-81, 1997.
9. "ASTM D 6115-97, Standard Test Method for Mode I Fatigue Delamination Growth Onset of Unidirectional Fiber-Reinforced Polymer Matrix Composites," in *Annual Book of ASTM Standards*. vol. 15.03: American Society for Testing and Materials, 2008.
10. P. Hansen and R. Martin, "DCB, 4ENF and MMB Delamination Characterisation of S2/8552 and IM7/8552," Materials Engineering Research Laboratory Ltd. (MERL), Hertford, UK N68171-98-M-5177, 1999.
11. "Standard Test Method for Mode I Fatigue Delamination Propagation of Unidirectional Fiber-Reinforced Polymer Matrix Composites," *draft standard*, ASTM International, Committee D30 on Composites, 2009.
12. "Fatigue Fracture Toughness," in *Composite Materials Handbook CMH-17*. Rev. G, Vol. 1, section 6.9.4, ASTM International, 2010.
13. Abaqus Analysis User's Manual, ABAQUS® Standard, Version 6.9, DSS Simulia, 2009.
14. Abaqus Theory Manual, ABAQUS® Standard, Version 6.9, DSS Simulia, 2009.
15. Abaqus Example Problems Manual, ABAQUS® Standard, Version 6.9, DSS Simulia, 2009.
16. M. L. Benzeggagh and M. Kenane, "Measurement of mixed-mode delamination fracture toughness of

unidirectional glass/epoxy composites with mixed-mode bending apparatus," *Composites Science and Technology*, vol. 56, pp. 439-449, 1996.

17. "KaleidaGraph: Data Analysis/Graphing Application for Macintosh and Windows Operating Systems," Synergy Software, 1996.

TABLE I. MATERIAL PROPERTIES [8].

Unidirectional Graphite/Epoxy Prepreg		
$E_{11} = 139.4 \text{ GPa}$	$E_{22} = 10.16 \text{ GPa}$	$E_{33} = 10.16 \text{ GPa}$
$\nu_{12} = 0.30$	$\nu_{13} = 0.30$	$\nu_{23} = 0.436$
$G_{12} = 4.6 \text{ GPa}$	$G_{13} = 4.6 \text{ GPa}$	$G_{23} = 3.54 \text{ GPa}$

The material properties are given with reference to the ply coordinate axes where index 11 denotes the ply principal axis that coincides with the direction of maximum in-plane Young's modulus (fiber direction). Index 22 denotes the direction transverse to the fiber in the plane of the lamina and index 33 the direction perpendicular to the plane of the lamina.

TABLE II. FRACTURE PARAMETERS.

Fracture Toughness Data [8] – Figure A1		
$G_{Ic} = 0.17 \text{ kJ/m}^2$	$G_{IIc} = G_{IIIc} = 0.49 \text{ kJ/m}^2$	$\eta = 1.62$
Delamination Growth Onset Data [10] – Figures 2, A3,		
$m_0 = 0.2023$	$m_I = -0.078924$	
Delamination Growth Rate Data (Paris Law) [8] – Figures 3, A5		
$G_{Ic} = 0.17 \text{ kJ/m}^2$	$G_{Ih} = 0.06 \text{ kJ/m}^2$	
$c = 2.44 \cdot 10^6$	$n = 10.61$	

APPENDIX

Delamination fatigue growth analysis in ABAQUS®

Delamination growth at the interfaces in laminated composites subjected to cyclic loadings can be simulated in ABAQUS® by specifying the low-cycle fatigue criterion propagation analysis using the direct cyclic approach [13]. The interface along which the delamination (or crack) propagates must be indicated in the model using a fracture criterion definition. The onset and growth of fatigue delamination at the interfaces are characterized by the relative fracture energy release rate. The fracture energy release rates at the crack tips in the interface elements are calculated based on the virtual crack closure technique (VCCT). The low-cycle fatigue analysis in ABAQUS® is a quasi-static analysis on a structure subjected to sub-critical cyclic loading. The low-cycle fatigue analysis in ABAQUS® uses the direct cyclic approach to obtain the stabilized cyclic response of the structure directly. The direct cyclic analysis uses a combination of Fourier series and time integration of the nonlinear material behavior to obtain the stabilized cyclic response of the structure iteratively and therefore avoids the numerical expense associated with a transient analysis. The direct cyclic analysis in ABAQUS® is therefore suited for very large problems in which many load cycles must be applied to obtain the stabilized response. The direct cyclic analysis in ABAQUS®, however, is limited to geometrically linear behavior and fixed contact conditions. The theory and algorithm to obtain a stabilized response using the direct cyclic approach are described in detail in the ABAQUS® Theory Manual [14].

Required input for ABAQUS®

The input required to perform a delamination onset and growth analysis in ABAQUS® Standard is discussed in the following paragraphs. It is assumed that the reader is familiar with ABAQUS® Standard and the syntax used in the input file (.inp). The focus is therefore on the specific input that relates to delamination propagation, low-cycle fatigue and the direct cyclic approach in ABAQUS®. Two example input files are given at the end of this appendix to provide an overview of an entire analysis and assist the readers in creating their own analyses.

Input for delamination propagation

The interface along which the delamination (or crack) propagates must be indicated in the model using a fracture criterion definition:

```
*DEBOND, SLAVE=VCCT_TOP, MASTER=VCCT_BOT, FREQ=1
*FRACTURE CRITERION, TYPE=fatigue, MIXED MODE BEHAVIOR=BK, TOLERANCE=<tol>
<c1>, <c2>, <c3>, <c4>, <r1>, <r2>, <GIc>, <GIIc>,
<GIIIc>, <eta>
```

where **VCCT_TOP** and **VCCT_BOT** are interface surfaces as shown in Figure A1 and **<tol>** is the tolerance within which the crack propagation criterion must be satisfied. The input parameters for the fracture criterion are obtained from the static mixed-mode failure criterion, the delamination growth onset criterion and the growth rate shown in Figures A2 –A5.

The critical energy release rates **<GIc>**, **<GIIc>**, **<GIIIc>** and the curve fit parameter **<eta>** are obtained from the mixed-mode failure criterion as shown in Figure A2. A quasi static mixed-mode fracture criterion is determined for a material by plotting the interlaminar fracture toughness, G_c , versus the mixed-mode ratio, G_{II}/G_T as shown in Figure A2. The fracture criterion is generated experimentally using pure Mode I ($G_{II}/G_T=0$) Double Cantilever Beam (DCB) tests (as shown in Figure 1) [7], pure Mode II ($G_{II}/G_T=1$) End-Notched Flexure (ENF) test, and Mixed Mode Bending (MMB) tests of varying ratios of G_I and G_{II} . For the material used in this study, the experimental

data (open, blue circles) and mean values (filled, blue circles) are shown in Figure A2 [8]. A 2D fracture criterion was suggested by Benzeggah and Kenane [16] using a simple mathematical relationship between G_c and G_{II}/G_T

$$G_c = G_{Ic} + (G_{IIc} - G_{Ic}) \cdot \left(\frac{G_{II}}{G_T} \right)^\eta \quad (\text{A1})$$

In this expression, G_{Ic} and G_{IIc} are the experimentally-determined fracture toughness data for mode I and II as shown in Figure A2. The factor η was determined by a curve fit using the Levenberg-Marquardt algorithm in the KaleidaGraphTM graphing and data analysis software [17].

The parameters **<c1>**, **<c2>** are obtained by solving the law for growth onset (shown in Figure A3) for the number of cycles N as shown in equation (8) and illustrated in Figure A4 (black curve). In the case where a law for growth onset is not available or immediate onset is desirable in the analysis, parameters such as suggested in the ABAQUS[®] example problem [15] may be chosen as shown in Figure A3 (red box and curve). The parameters **<c3>**, **<c4>** are obtained directly from the Paris Law as shown in Figure A5. The parameter **<r1>** is calculated from the energy release rate cutoff value, G_{th} , and the fracture toughness, G_{Ic} , as shown in Figure A5. To calculate the parameter **<r2>** the user needs to define an energy release rate upper limit, G_{pl} , above which the fatigue crack will grow at an accelerated rate as shown in Figure A5. For the current benchmark example, G_{pl} was chosen to be 90% of the fracture toughness.

Input for cyclic loading

Defining a low-cycle fatigue analysis using the direct cyclic approach in ABAQUS[®] Standard requires the definition of an amplitude curve which describes the relative load magnitude:

```
*amplitude,name=test, DEFINITION=PERIODIC
<n>,<omega>,<t_0>,<A_0>
<A_1>,<B_1>
```

where **test** is the label to be used to refer to the amplitude curve. The parameters defined in the first line are the number of terms in the Fourier series, **<n>**, the circular frequency, **<omega>**, in radians per time, the starting time, **<t₀>**, and the constant term in the Fourier series, **<A₀>**, as shown in Figure A6. The parameters defined in the second line are the first coefficient of the cosine terms, **<A₁>**, and the first coefficient of the sine terms, **<B₁>**, also shown in Figure A6.

The amplitude curve is then referenced in the definition of the cyclic loading. In the current example, prescribed displacements were used to simulate the cyclic opening of the arms of the DCB specimen:

```
*BOUNDARY,AMPLITUDE=test
LFRONTP, 1, 1, 0.67
LFRONTM, 1, 1, -0.67
```

where **LFRONTP** and **LFRONTM** are node sets located at the tip of each arm where the displacements are applied as shown in Figure A1. The factor **0.67** is used to multiply the relative magnitude defined by the amplitude curve (shown in Figure A6) and obtain the applied cyclic displacement, $\delta/2$, as shown in Figure A7.

The direct cyclic approach in ABAQUS[®] Standard is used to obtain the stabilized cyclic response of a structure directly:

```

*direct cyclic,fatigue
<i0>,<ts>,,,<ni>,<nmax>,<Δn>,<imax>,
,,<NT>,

```

where the parameter **fatigue** is used to perform a low-cycle fatigue analysis. The parameters defined in the first line are the initial time increment, $\langle i_0 \rangle$, the time of a single loading cycle, $\langle t_s \rangle$ (as shown in Figure A7), the minimum time increment allowed (not used), the maximum time increment allowed (not used), the initial number of terms in the Fourier series, $\langle n_i \rangle$, the maximum number of terms in the Fourier series, $\langle n_{max} \rangle$, the increment in number of terms in the Fourier series, $\langle \Delta n \rangle$, and the maximum number of iterations allowed in a step, $\langle i_{max} \rangle$. The parameters defined in the second line are the minimum increment in number of cycles over which the damage is extrapolated forward (default used), the maximum increment in number of cycles over which the damage is extrapolated forward (default used), the total number of cycles allowed in a step, $\langle N_T \rangle$, and the damage extrapolation tolerance (default used). The time of a single loading cycle was kept constant at $t_s=0.1$ s for all analyses. Most analyses were run up to $N_T=10^7$ cycles in order to reach the threshold after which delamination growth stops as shown in Figures 11 and 12. All other input parameters were varied and the effect on the results studied as discussed in the main part of this report.

Control parameters direct cyclic analysis

Solution controls in ABAQUS[®] Standard can be reset and modified by using keyword

```

*controls,type=direct cyclic
<Ipr>,<CRn>,<CUn>,<CR0>,<CU0>,

```

where the parameter **direct cyclic** is used to set parameters that will be used to control the stabilized state and plastic ratcheting detections and to specify when to impose the periodicity condition for direct cyclic analysis. If this keyword is omitted, default parameters are used. The parameters defined in the first line are the iteration number at which the periodicity condition is first imposed, $\langle I_{pr} \rangle$, (default used), the stabilized state detection criterion for the ratio of the largest residual coefficient on any terms in the Fourier series to the corresponding average flux norm, $\langle CR_n \rangle$, the stabilized state detection criterion for the ratio of the largest correction to the displacement coefficient on any terms in the Fourier series to the largest displacement coefficient, $\langle CU_n \rangle$, plastic ratcheting detection criterion for the ratio of the largest residual coefficient on the constant term in the Fourier series to the corresponding average flux norm, $\langle CR_0 \rangle$, and the plastic ratcheting detection criterion for the ratio of the largest correction to the displacement coefficient on the constant term in the Fourier series to the largest displacement coefficient, $\langle CU_0 \rangle$ [13]. These control parameters were varied and the effect on the results studied as discussed in the main part of this report.

Example input files

Two example input files are given to provide an overview of an entire analysis and assist the readers in creating their own analyses. The analysis was divided into two steps. In the first step, a small static preload step was introduced as a work around to avoid problems discovered with the initial contact conditions (ABAQUS[®] bug v68_1987). The second step was set-up to perform the desired cyclic analysis. It was found that the prescribed displacements in the static preload step had to be small (0.0067 mm) compared to the prescribed displacements ($\delta_{min}/2=0.067$, $\delta_{max}/2=0.67$) which were used to simulate the cyclic opening of the arms of the DCB specimen.

Analyses where larger preload steps were chosen did not converge in the second step and terminated prematurely.

For all analyses, the input to define the fracture criterion (**<GIc>**, **<GIIC>**, **<GIIIc>**, **<eta>**), the parameters for delamination onset (**<c1>**, **<c2>**), and delamination growth (Paris Law) (**<c3>**, **<c4>**, **<r1>**, **<r2>**) were kept constant. The parameters to define the load frequency (**<omega>**, **<A₀>**) as well as the minimum and maximum applied displacement (**<t_s>**, $\delta_{max}/2=0.67$) were also kept constant during all analyses. Other parameters required to define the Fourier series which is used to define the cyclic load, the initial time increment and the optional input parameters to control the solution in ABAQUS[®] Standard were varied. The ABAQUS[®] keywords shown in **bold type** were discussed in detail in the previous paragraphs.

Input file for fatigue onset and growth analysis

```

*HEADING
DCB-UD-T300/1076, a=30.5 mm
units: mm, N, MPa
*** elements, nodes, material, etc
...
...
*NSET, NSET=BONDED, GENERATE
    253, 1693, 8
**** surface and contact definition for VCCT ****
*SURFACE, TYPE=ELEMENT, NAME=VCCT_BOT
    EL_BOT, S3
*SURFACE, TYPE=ELEMENT, NAME=VCCT_TOP
    EL_TOP, S1
*CONTACT PAIR, INTERACTION=VCCT, ADJUST=BONDED, small sliding
    VCCT_TOP, VCCT_BOT
*SURFACE INTERACTION, NAME=VCCT
    <width>
*INITIAL CONDITION, TYPE=CONTACT
    VCCT_TOP, VCCT_BOT, BONDED
**
*NSET, NSET=LFRONTTP
    8
*NSET, NSET=LFRONTM
    1
**** VCCT fatigue input
*parameter
** Damage and tolerance parameters
tol=0.001
** Fracture toughness:
GIc = 0.17030
GIIC = 0.49360
GIIIc = 0.5
** B-K parameter:
eta=1.62
** width in the plane stress/strain direction
width =25.0
** fatigue crack growth data **
c1=2.8E-09
c2=-12.415
c3=2.44E+06
c4=10.61

```

```

r1=0.353
r2=0.9
***
*** amplitude ****
*amplitude,name=test, DEFINITION=PERIODIC
1,62.832,0.,0.55
0,0.45
*** history data ***
*** static ramp up step ****
*STEP, NLGEOM, INC= 10000
*STATIC
0.001, 0.001
**
*DEBOND,SLAVE=VCCT_TOP,MASTER=VCCT_BOT,FREQ=1
*FRACTURE CRITERION,TYPE=VCCT,MIXED MODE BEHAVIOR=BK
1.0e6,1.0e6,1.0e6,<eta>
**
*BOUNDARY, TYPE=DISPLACEMENT
LFRONTP, 1, 1, 0.00067
LFRONTM, 1, 1, -0.00067
** field and history output **
*OUTPUT, FIELD, VARIABLE=PRESELECT, FREQ=1
*Output, history,VARIABLE=PRESELECT,freq=1
*NODE output,NSET=LFRONTP
RF1
*NODE output,NSET=LFRONTP
U1
*END STEP
*STEP, INC= 10000
*direct cyclic,fatigue
0.001,0.1,,,11,11,5,10,
,,10000000,,
*DEBOND,SLAVE=VCCT_TOP,MASTER=VCCT_BOT,FREQ=1
*FRACTURE CRITERION,TYPE=fatigue,MIXED MODE BEHAVIOR=BK, TOLERANCE=<tol>
<c1>,<c2>,<c3>,<c4>,<r1>,<r2>,<G1c>,<GIIc>,
<GIIIc>,<eta>
*** run analysis first with default values
*controls,type=direct cyclic
,100,5.E-3,5.E-3,5.E-3
*BOUNDARY,AMPLITUDE=test
LFRONTP, 1, 1, 0.67
LFRONTM, 1, 1, -0.67
**
** field and history output **
*OUTPUT, FIELD, VARIABLE=
*ELEMENT OUTPUT
cycleini,status,sdeg
*CONTACT OUTPUT, MASTER=VCCT_BOT, SLAVE=VCCT_TOP
dbt,dbsf,dbs,openbc,crsts,enrrt,efenrrtr,bdstat
*Output, history,VARIABLE=PRESELECT,freq=25
*NODE output,NSET=LFRONTP
RF1
*NODE output,NSET=LFRONTP
U1
*END STEP

```

Input file to verify correct input data and model response

It is recommended to perform a static analysis first, to verify the correct input parameters. A single cycle is performed by replacing the input for direct cyclic analysis

```
*direct cyclic,fatigue
  0.001,0.1,,,11,11,5,10,
,,1000000,,
```

in the second step with

```
*STATIC
  0.001, 0.1, 1.E-10, 0.001
```

By monitoring the applied displacements, $\delta/2$, during the simulation, the input data for the cyclic analysis can be checked as shown in the example in Figure A8. For all analysis shown, the first step consisted of a static preload step up to $\delta/2=0.00067$. In the second step, the number of terms in the Fourier series, $\langle n \rangle$, the circular frequency, $\langle \omega \rangle$, the constant term in the Fourier series, $\langle A_0 \rangle$, and the time of a single loading cycle, $\langle t_s \rangle$ were kept the same for all analyses. Further, the factor **0.67** used to multiply the relative magnitude defined by the amplitude curve to obtain the applied displacement, $\delta/2$, was kept constant. The applied displacement, $\delta/2$, therefore varied between $\delta_{max}/2=0.67$ mm and $\delta_{min}/2=0.067$ mm at a frequency of 10 Hz as desired. As an example, the starting time, $\langle t_0 \rangle$, the first coefficient of the cosine terms, $\langle A_1 \rangle$, and the first coefficient of the sine terms, $\langle B_1 \rangle$, were varied to create different sine waves (in red) and cosine waves (in blue) with the same displacement maximum, minimum and frequency as shown in Figure A8.

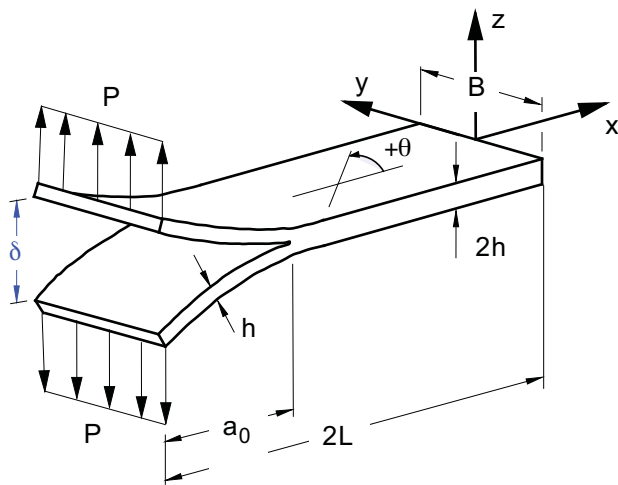
```
*HEADING
DCB-UD-T300/1076, a=30.5 mm
units: mm, N, MPa
*** elements, nodes, material, etc
...
...
*NSET, NSET=BONDED, GENERATE
  253, 1693, 8
**** surface and contact definition for VCCT ****
*SURFACE, TYPE=ELEMENT, NAME=VCCT_BOT
  EL_BOT, S3
*SURFACE, TYPE=ELEMENT, NAME=VCCT_TOP
  EL_TOP, S1
*CONTACT PAIR, INTERACTION=VCCT, ADJUST=BONDED, small sliding
  VCCT_TOP, VCCT_BOT
*SURFACE INTERACTION, NAME=VCCT
  <width>
*INITIAL CONDITION, TYPE=CONTACT
  VCCT_TOP, VCCT_BOT, BONDED
**
*NSET, NSET=LFRONTP
  8
*NSET, NSET=LFRONTM
  1
**** VCCT fatigue input
*parameter
** Damage and tolerance parameters
tol=0.001
** Fracture toughness:
```

```

GIIc = 0.17030
GIIIc = 0.49360
GIIIc = 0.5
** B-K parameter:
eta=1.62
** width in the plane stress/strain direction
width =25.0
** fatigue crack growth data **
c1=2.8E-09
c2=-12.415
c3=2.44E+06
c4=10.61
r1=0.353
r2=0.9
***
*** amplitude ****
*amplitude,name=test, DEFINITION=PERIODIC
1,62.832,0.,0.55
0,0.45
*** history data ***
*** static ramp up step ****
*STEP, NLGEOM, INC= 10000
*STATIC
0.001, 0.1
**
*DEBOND,SLAVE=VCCT_TOP,MASTER=VCCT_BOT,FREQ=1
*FRACTURE CRITERION,TYPE=VCCT,MIXED MODE BEHAVIOR=BK
1.0e6,1.0e6,1.0e6,<eta>
**
*BOUNDARY, TYPE=DISPLACEMENT
LFRONTP, 1, 1, 0.067
LFRONTM, 1, 1, -0.067
** field and history output **
*NODE PRINT, NSET=BONDED, GLOBAL=YES, FREQ=1
COORD
*OUTPUT, FIELD, VARIABLE=PRESELECT, FREQ=1
*Output, history,VARIABLE=PRESELECT,freq=1
*NODE output,NSET=LFRONTP
RF1
*NODE output,NSET=LFRONTP
U1
*CONTACT OUTPUT, MASTER=VCCT_BOT, SLAVE=VCCT_TOP,NSET=BONDED
dbt,enrrt,bdstat
*END STEP
*STEP, NLGEOM, INC= 10000
*** run static analysis with one cycle first to verify input
*STATIC
0.001, 0.1, 1.E-10, 0.001
*DEBOND,SLAVE=VCCT_TOP,MASTER=VCCT_BOT,FREQ=1
*FRACTURE CRITERION,TYPE=VCCT,MIXED MODE BEHAVIOR=BK
1.0e6,1.0e6,1.0e6,<eta>
*BOUNDARY,AMPLITUDE=test
LFRONTP, 1, 1, 0.67
LFRONTM, 1, 1, -0.67
**
** field and history output **
*OUTPUT, FIELD, VARIABLE=PRESELECT, FREQ=1
*ELEMENT OUTPUT

```

```
status
*CONTACT OUTPUT, MASTER=VCCT_BOT, SLAVE=VCCT_TOP
  dbt,dbsf,dbs,openbc,crsts,enrrt,efenrrtr,bdstat
*Output, history,VARIABLE=PRESELECT,freq=1
*NODE output,NSET=LFRONTP
  RF1
*NODE output,NSET=LFRONTP
  U1
*CONTACT OUTPUT, MASTER=VCCT_BOT, SLAVE=VCCT_TOP,NSET=BONDED
  dbt,enrrt,bdstat
*END STEP
```



dimensions

B	25.0 mm
2h	3.0 mm
2L	150.0 mm
a_0	30.5 mm

fatigue loading

$\delta_{max}/2$	0.67 mm
$\delta_{min}/2$	0.067 mm
R	0.1
f	10.0 Hz

layup: $[0]_{24}$

Figure 1. *Double Cantilever Beam Specimen (DCB)*

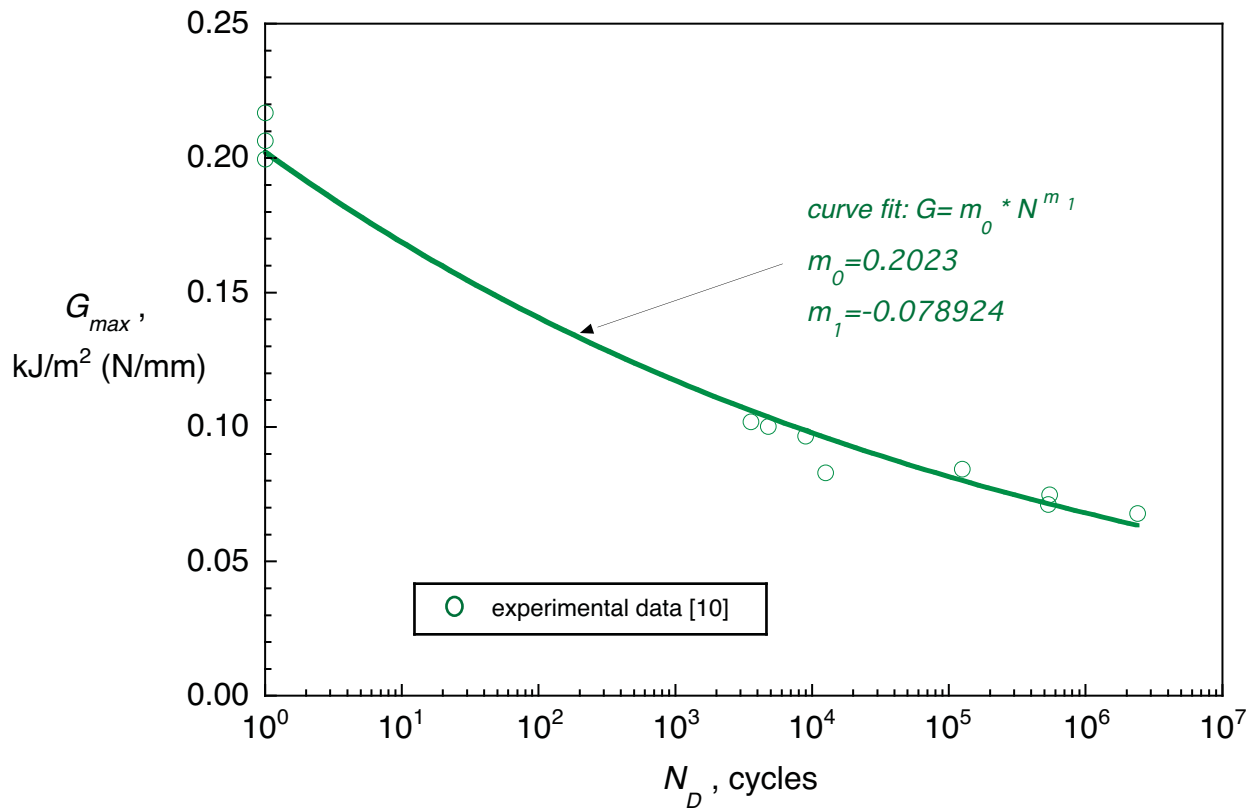


Figure 2. *Delamination growth onset for DCB specimen.*

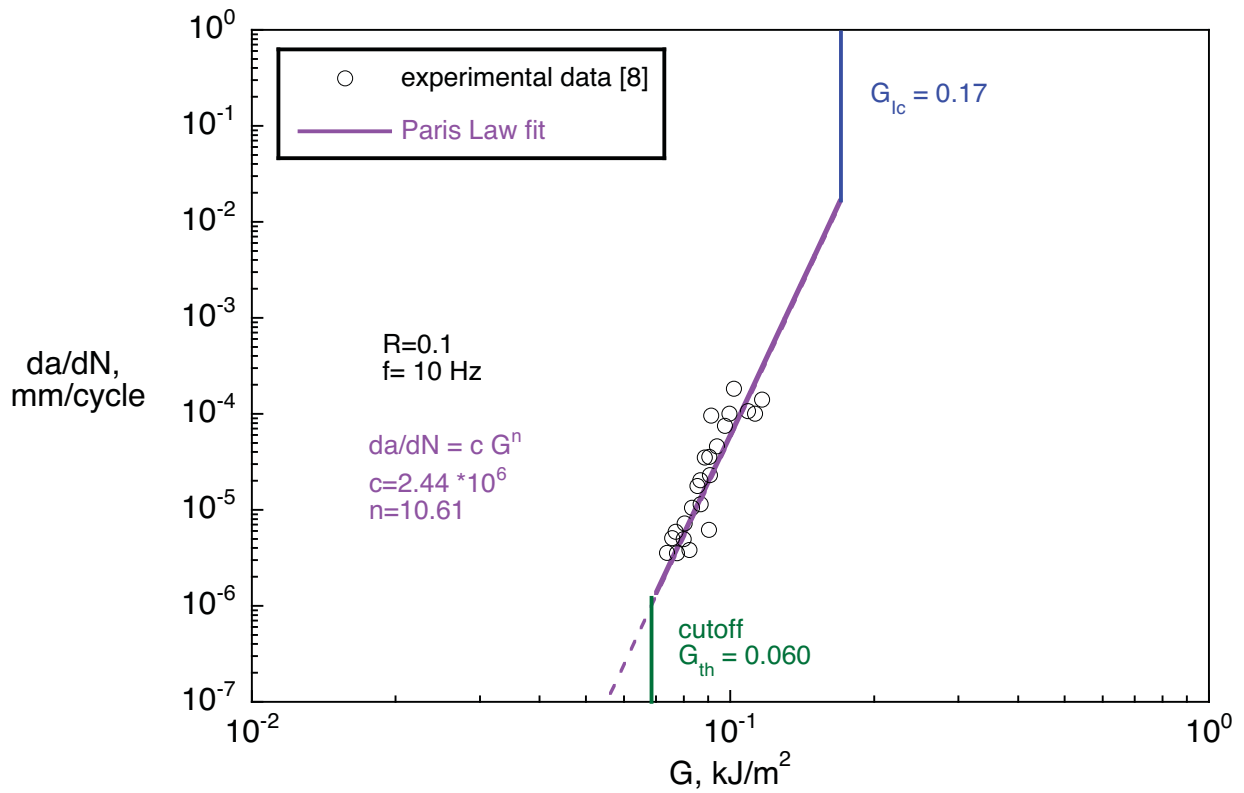


Figure 3. Delamination growth rate (Paris Law) [8].

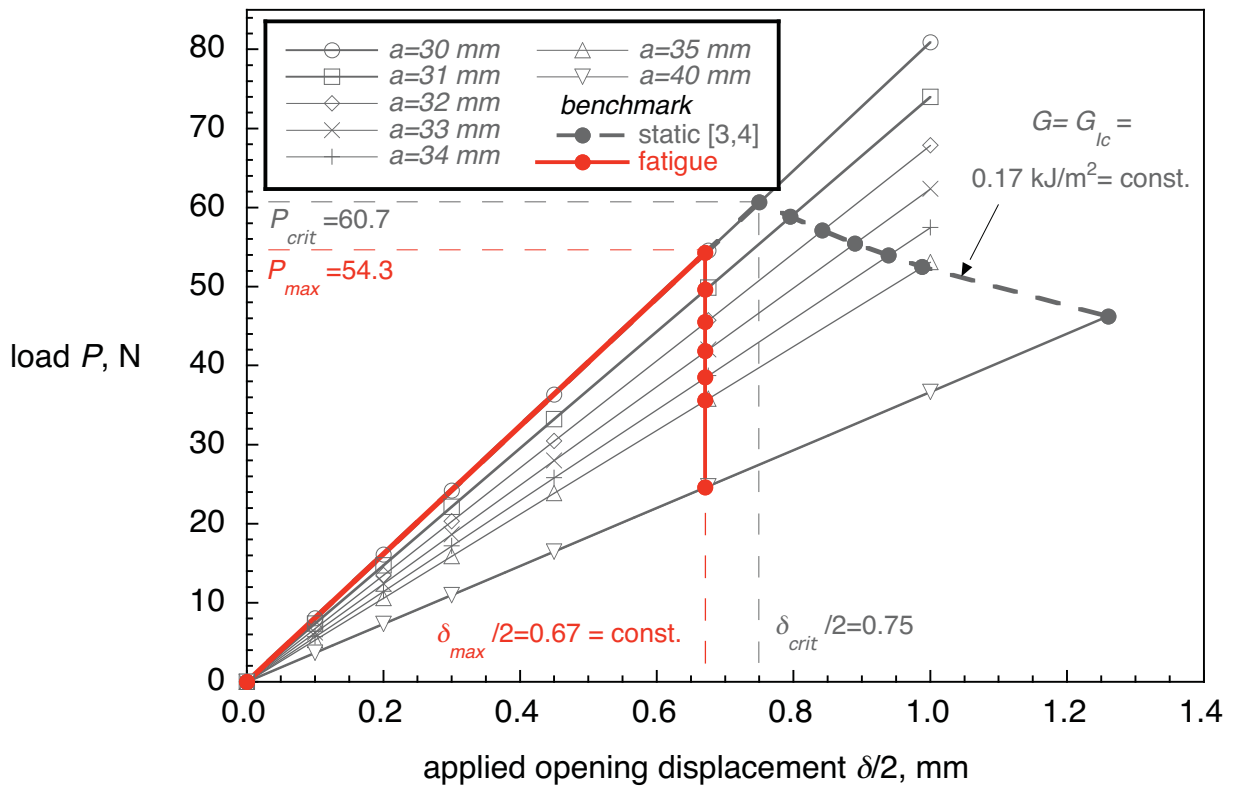


Figure 4. Critical load-displacement behavior for a DCB specimen.

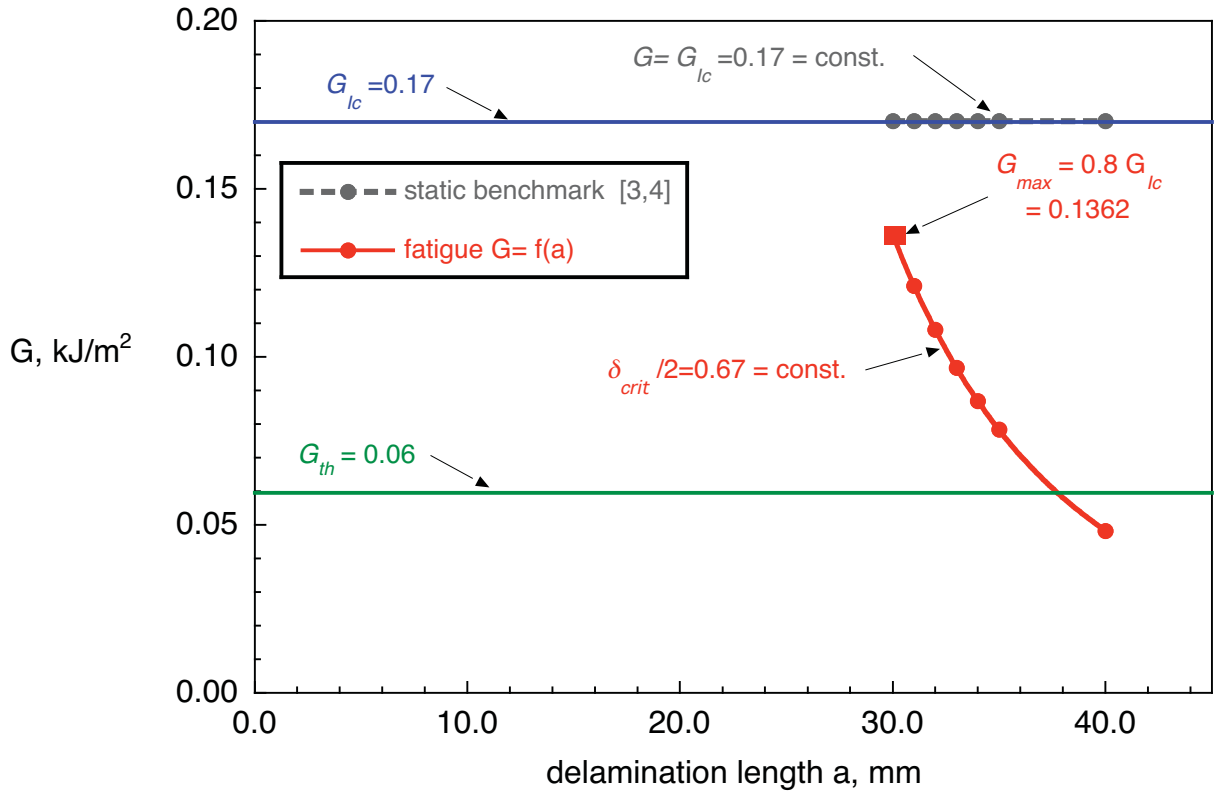


Figure 5. Energy release rate - delamination length behavior for DCB specimen.

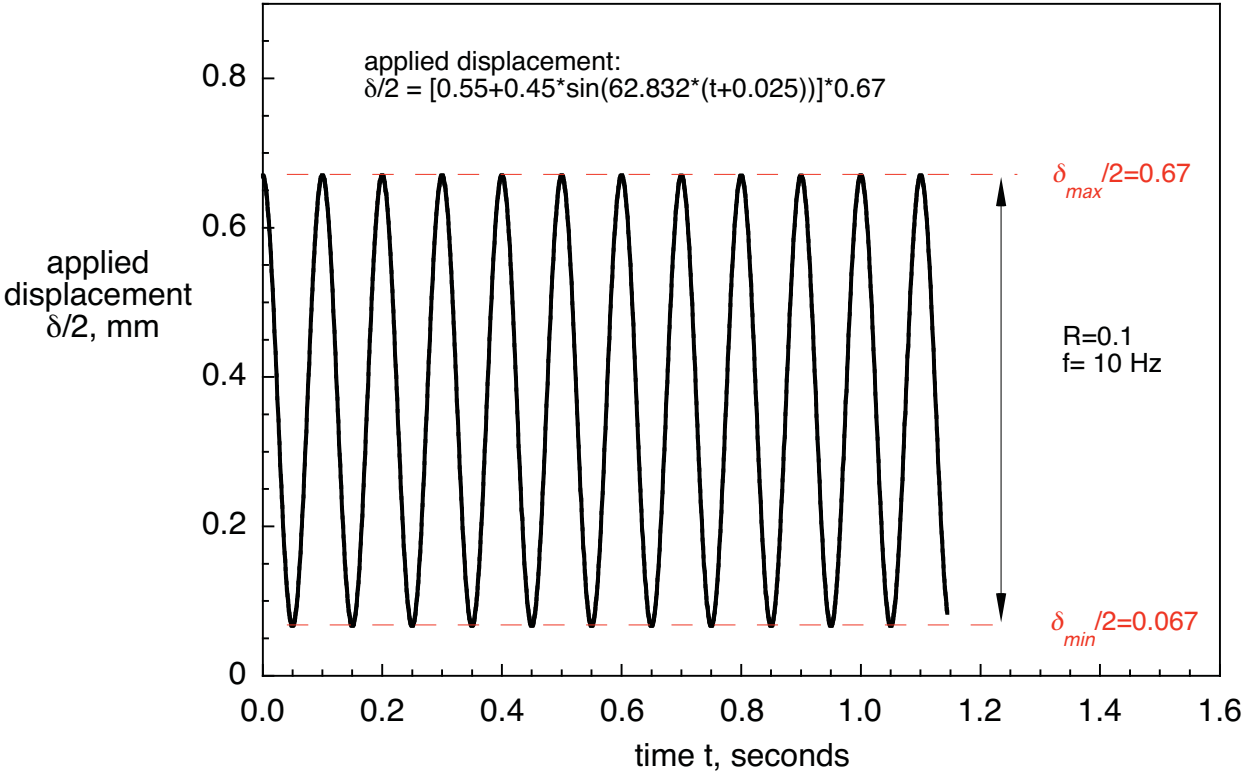
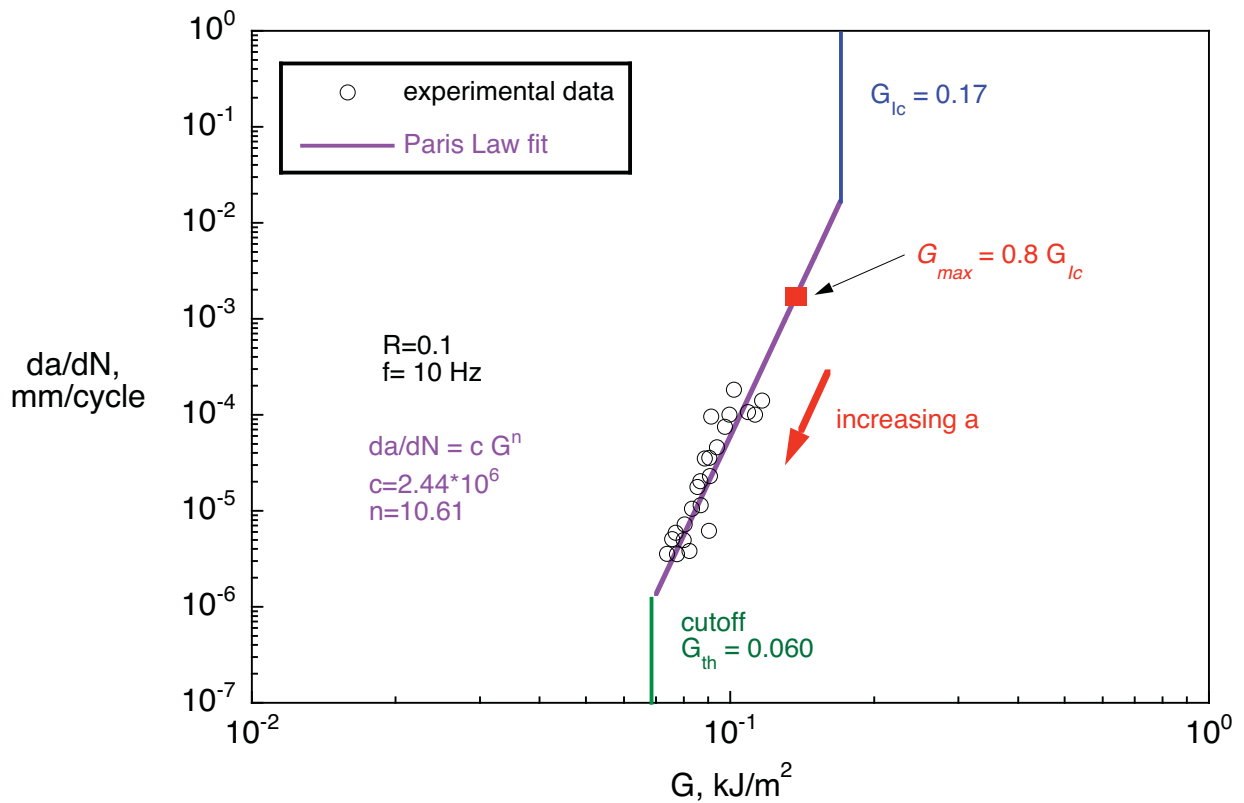
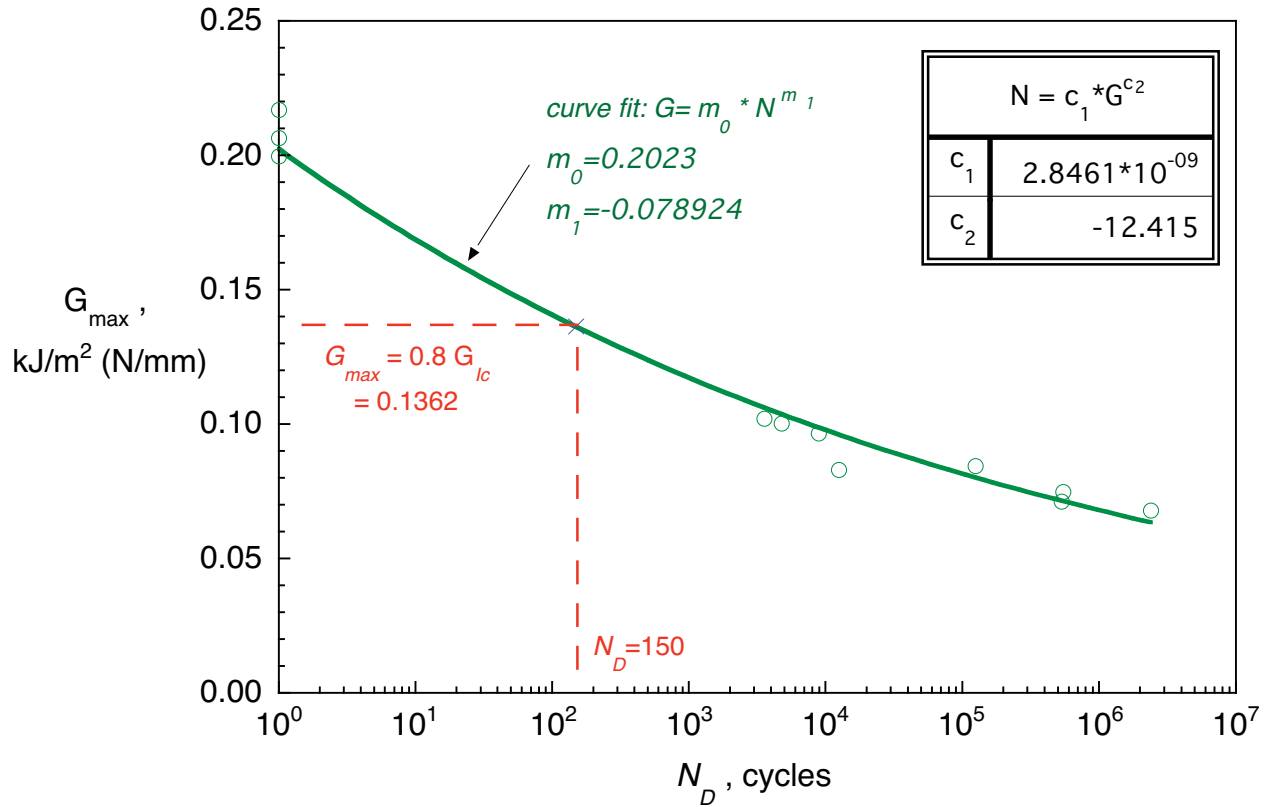


Figure 6. Cyclic fatigue loading for DCB specimen.



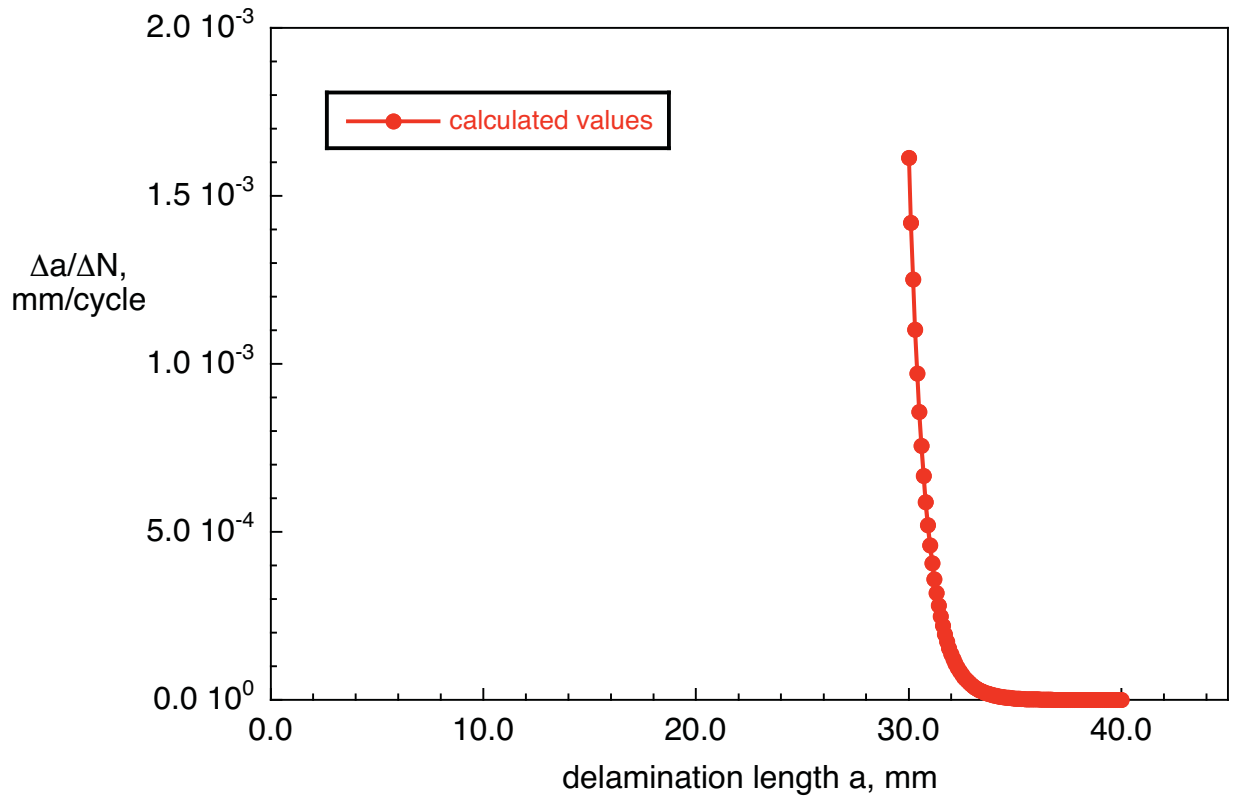


Figure 9. Delamination growth rate behavior for DCB specimen.

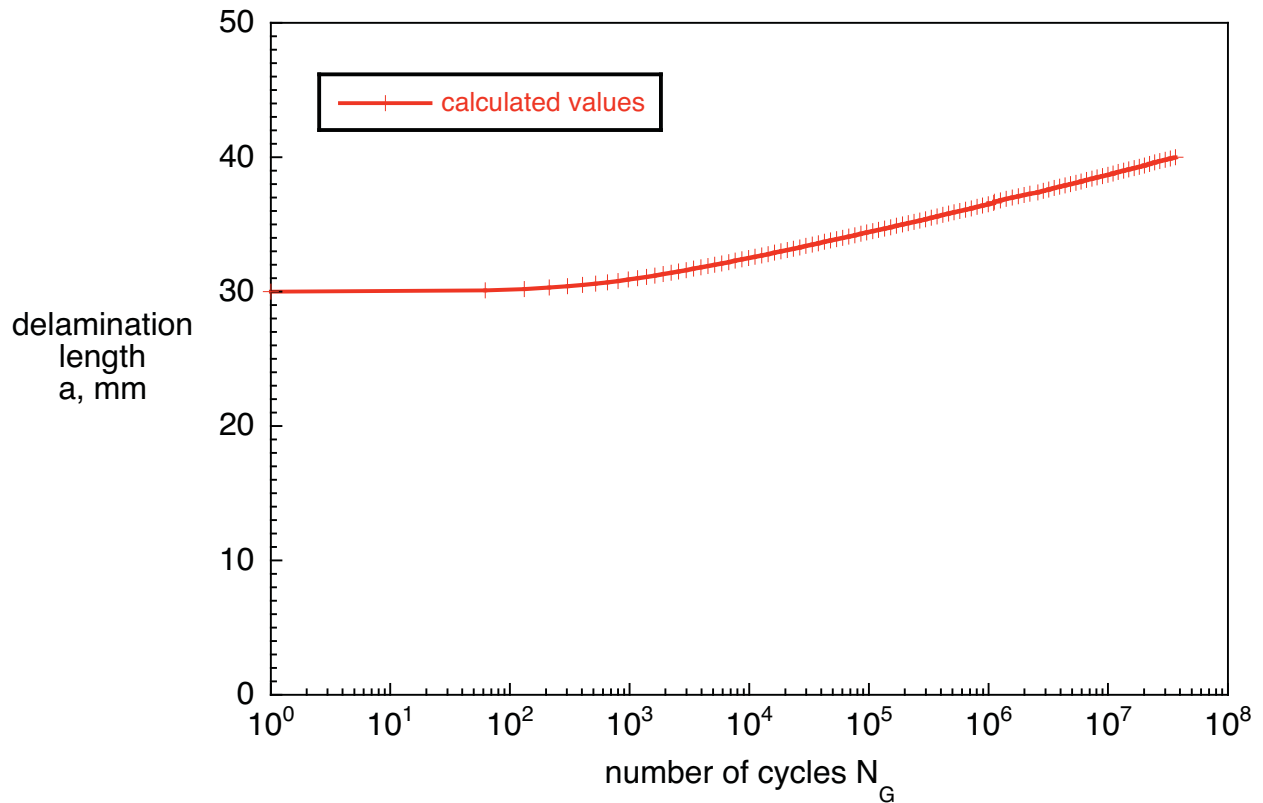


Figure 10. Stable delamination growth behavior for DCB specimen.

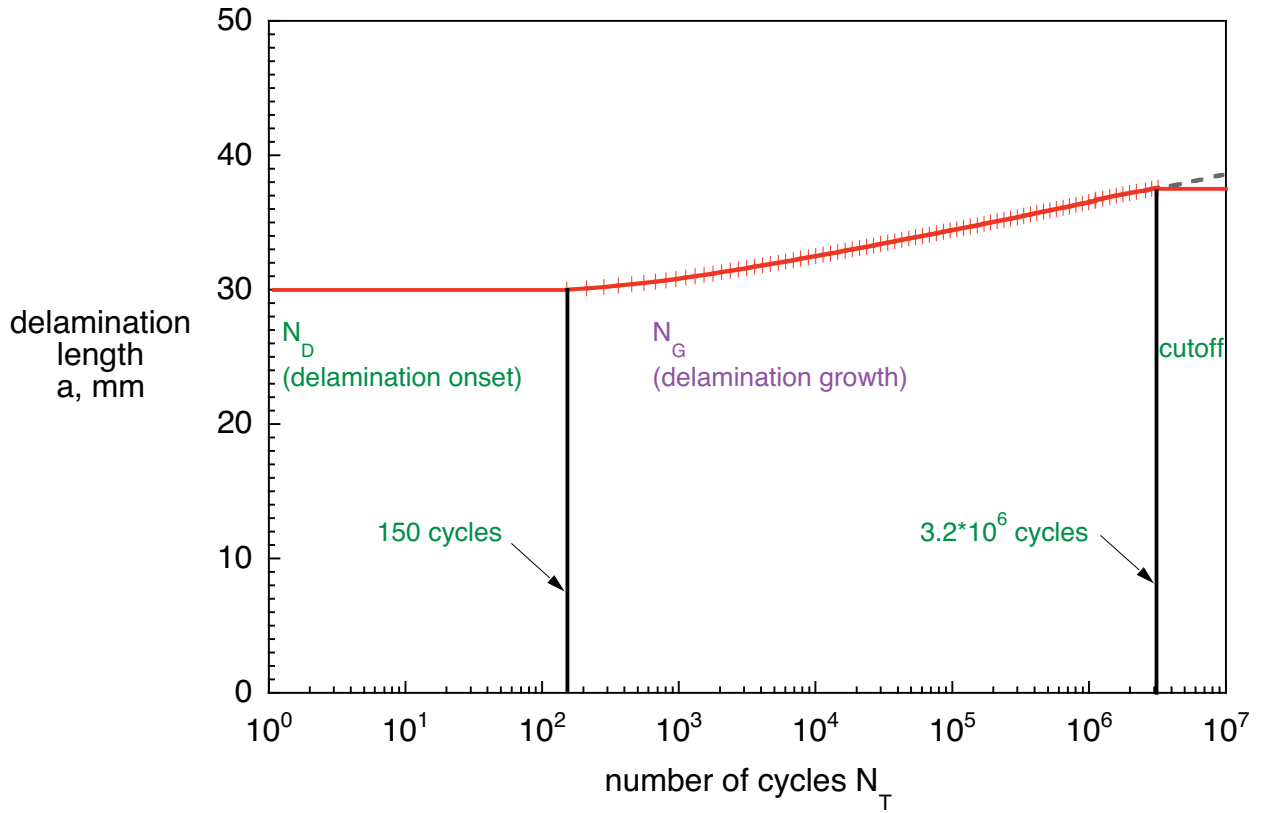


Figure 11. Delamination onset and growth behavior for DCB specimen.

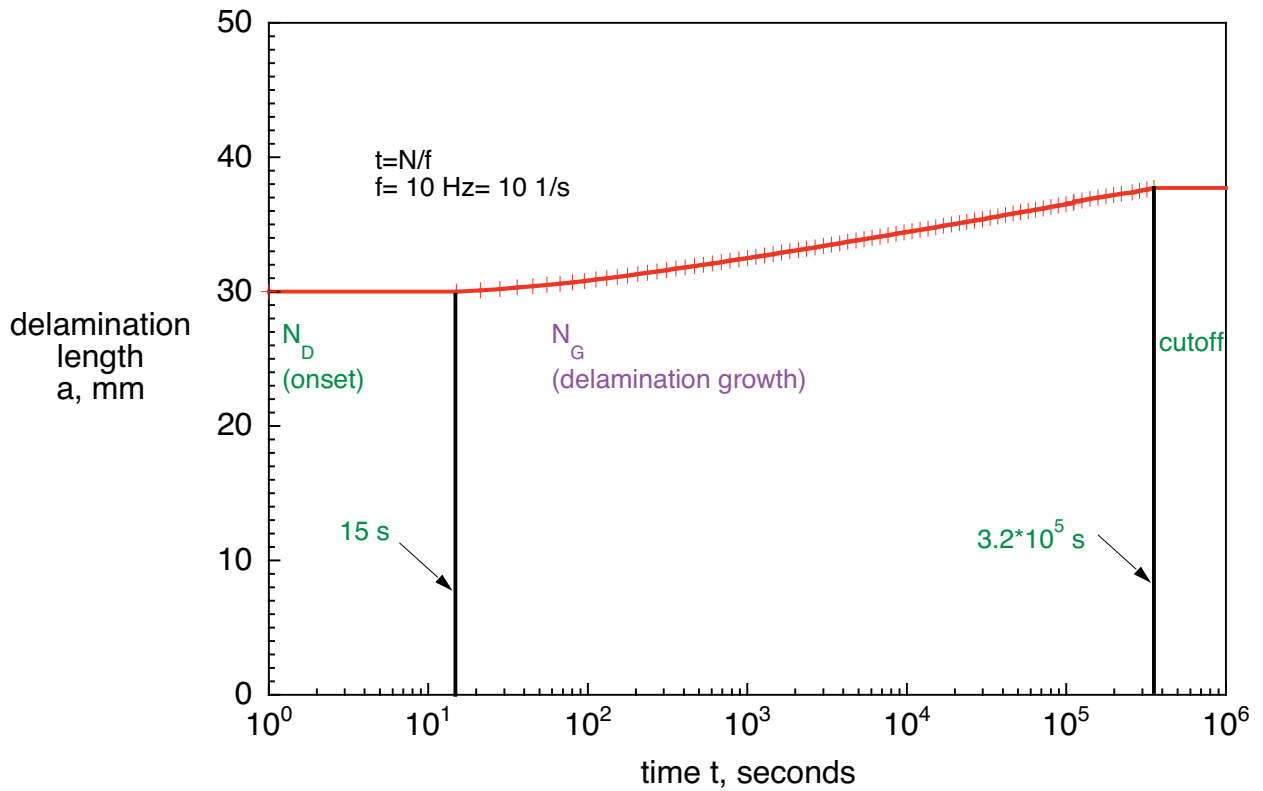
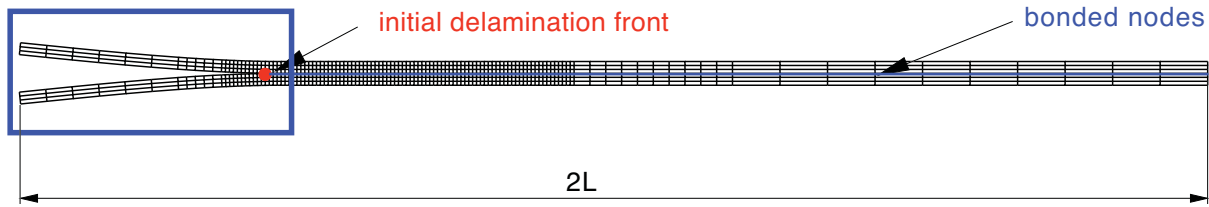
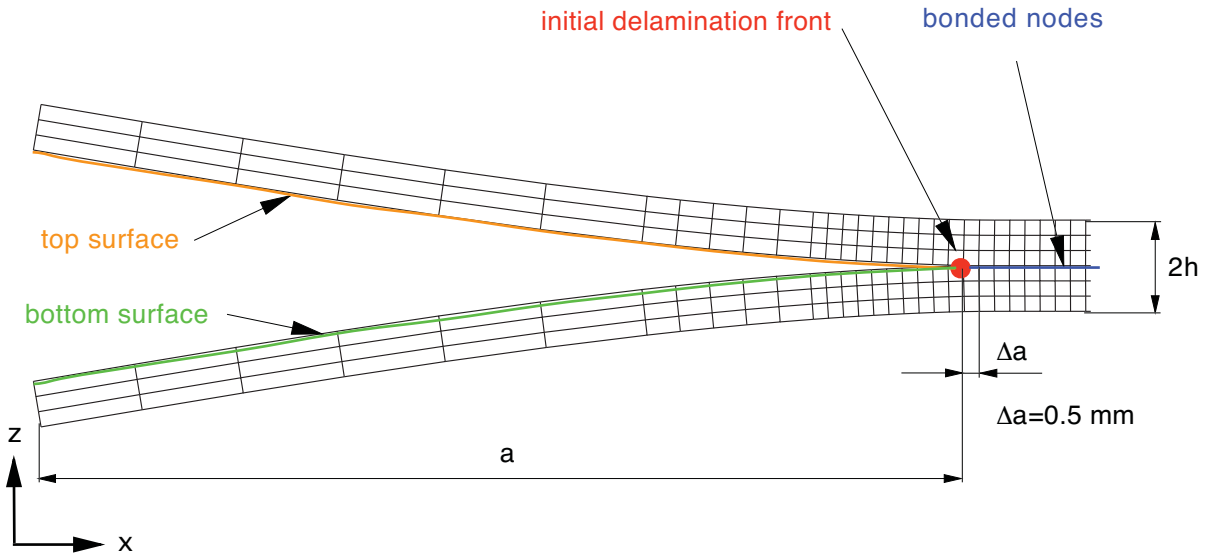


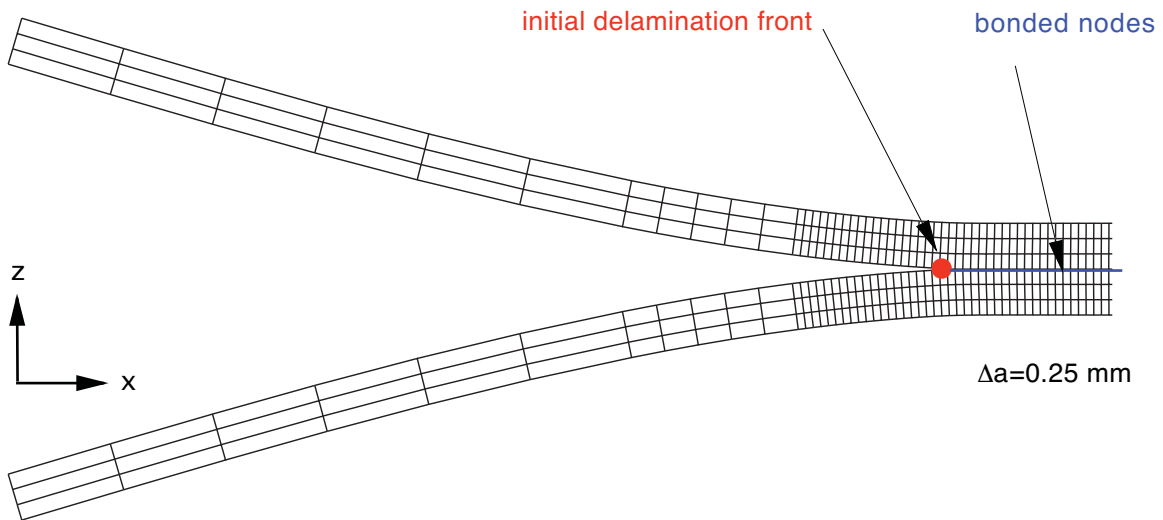
Figure 12. Delamination onset and growth behavior for DCB specimen.



a. Deformed FE-model of DCB specimen with initial delamination before growth

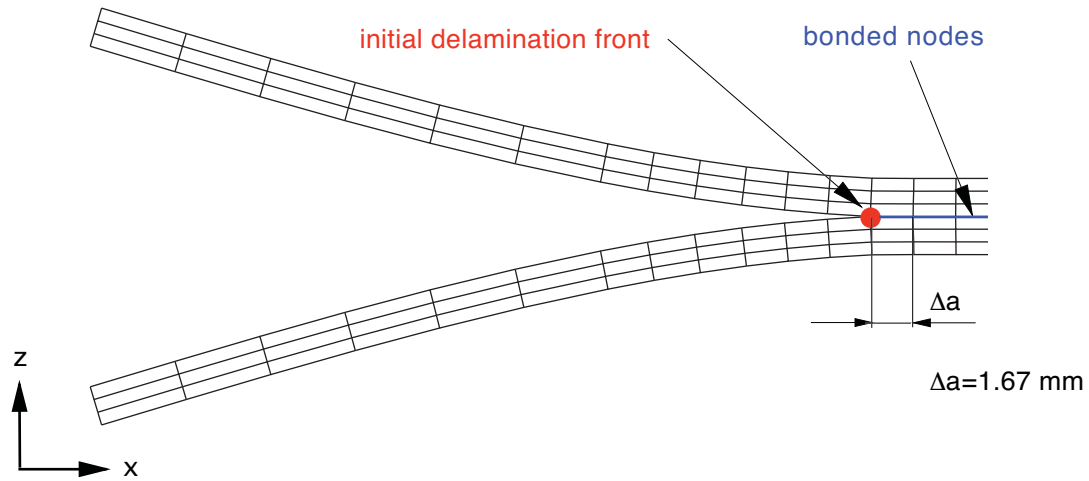


b. Detail of a FE-model of a DCB specimen

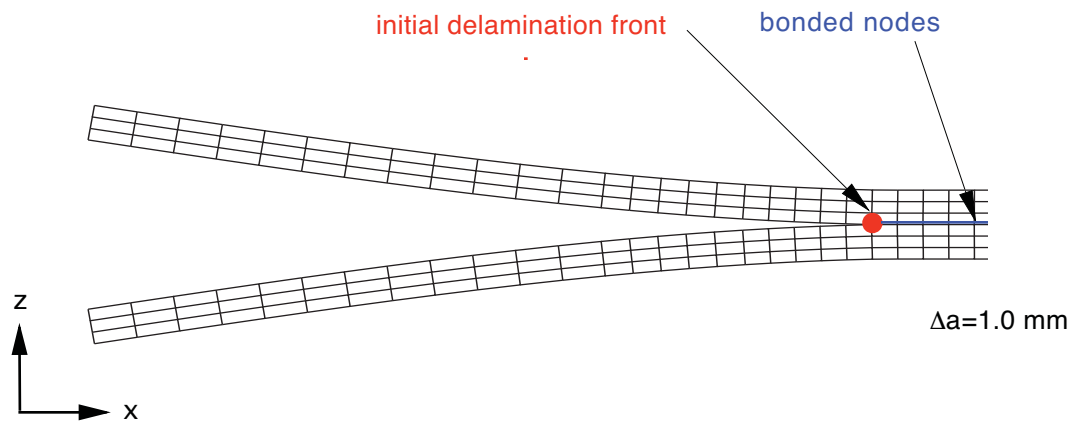


c. Detail of a refined FE-model of a DCB specimen

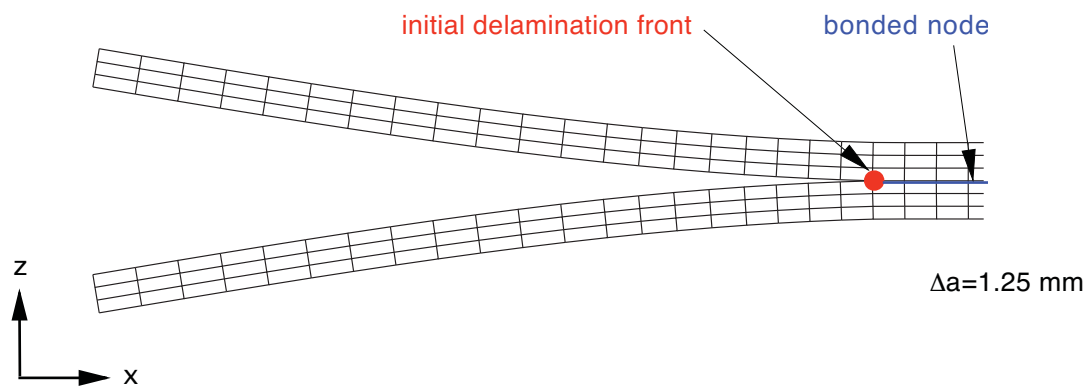
Figure 13. Two-dimensional finite element model of a DCB specimen.



a. Detail of a FE-model of a DCB specimen

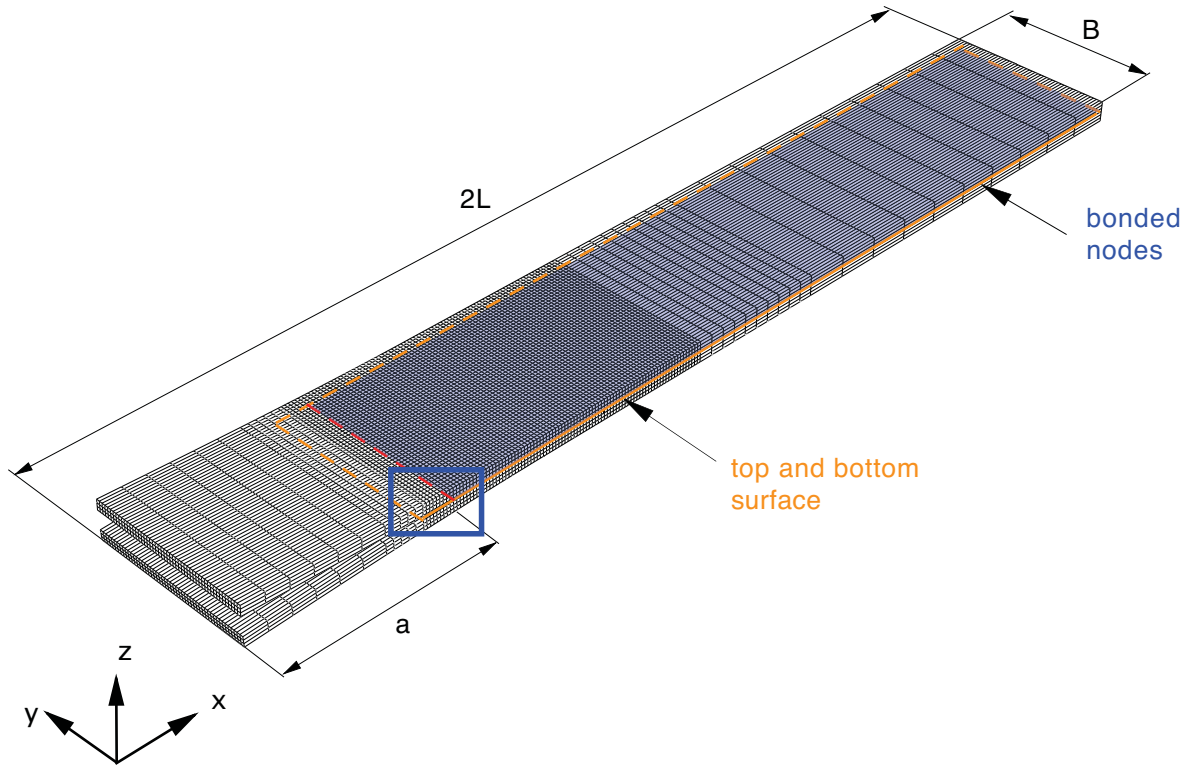


b. Detail of a FE-model of a DCB specimen

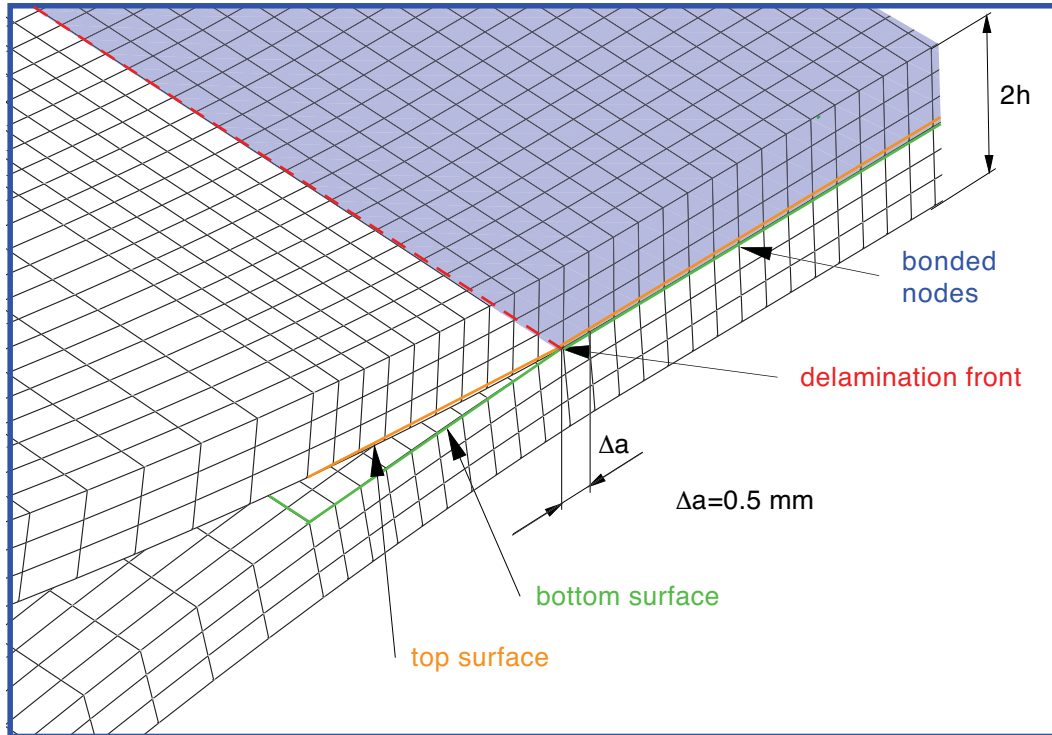


c. Detail of a refined FE-model of a DCB specimen

Figure 14. Details of different two-dimensional finite element models of a DCB specimen.

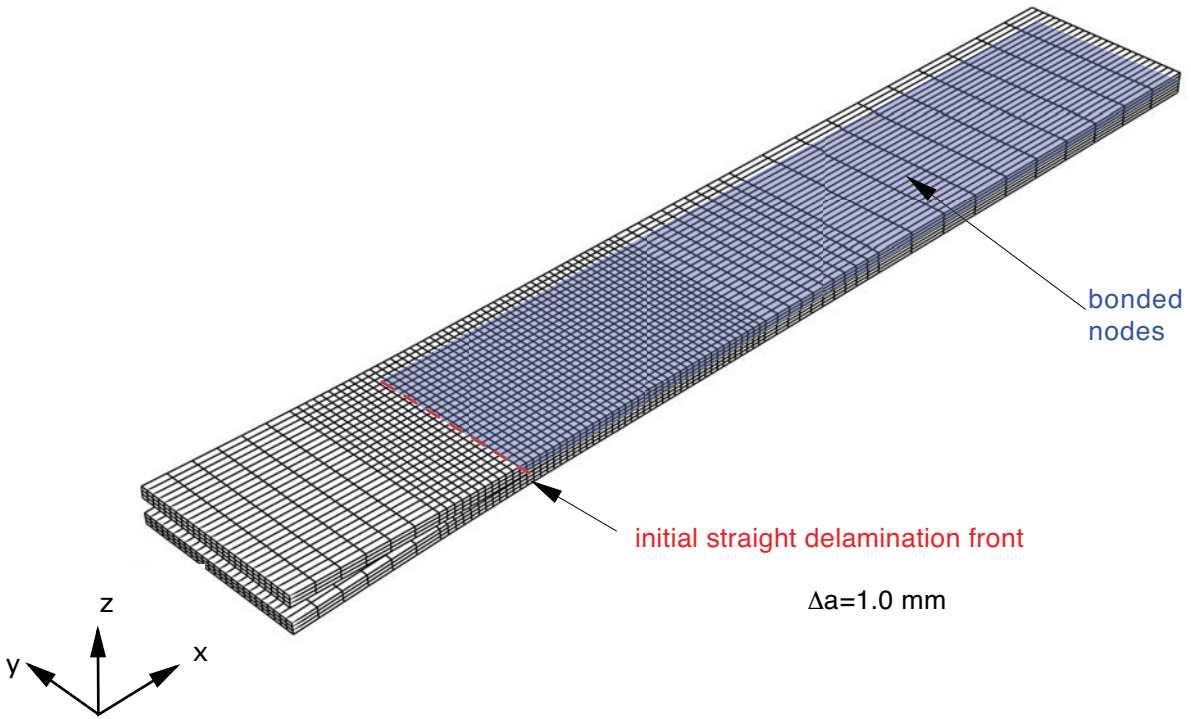


a. Deformed three-dimensional FE-model with initial delamination front before growth

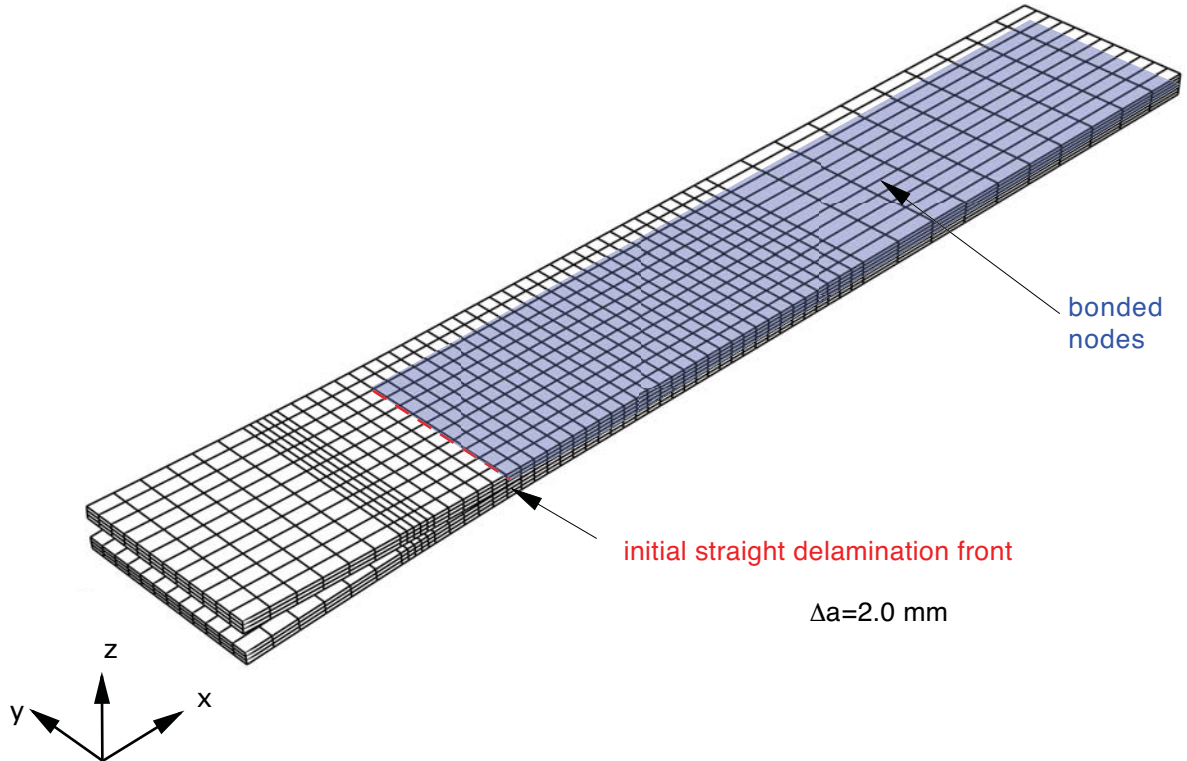


b. Detail of three-dimensional FE-model around delamination front

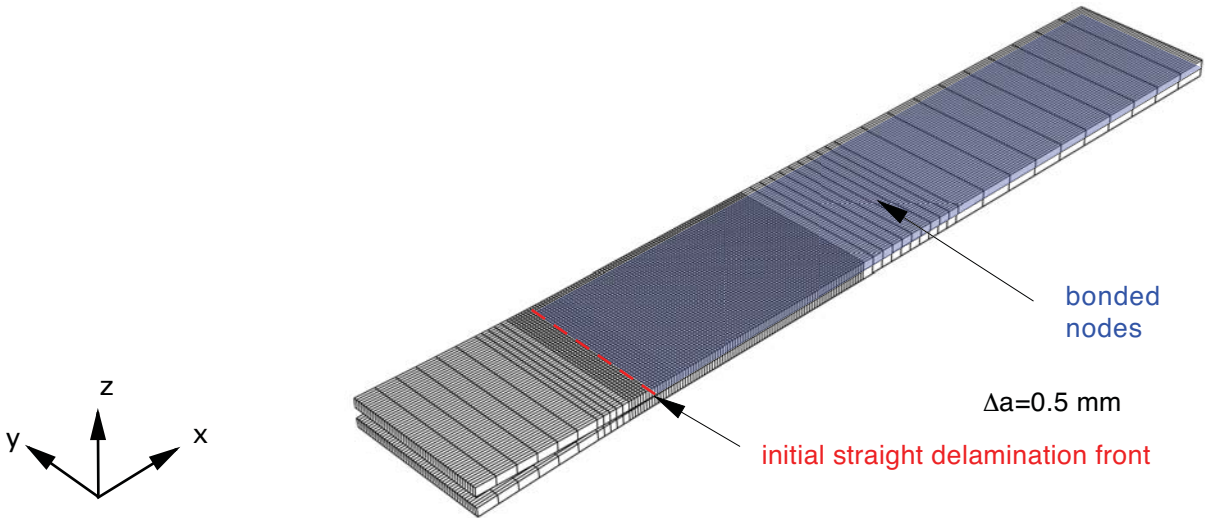
Figure 15. Full three-dimensional finite element model of a DCB specimen.



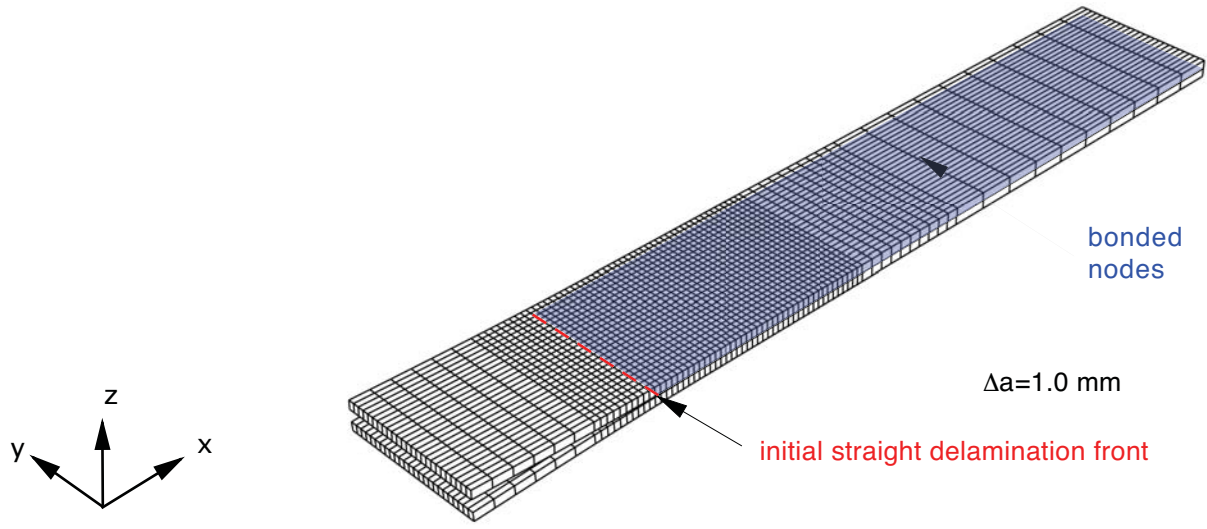
a. Deformed three-dimensional model of DCB specimen with a coarse mesh



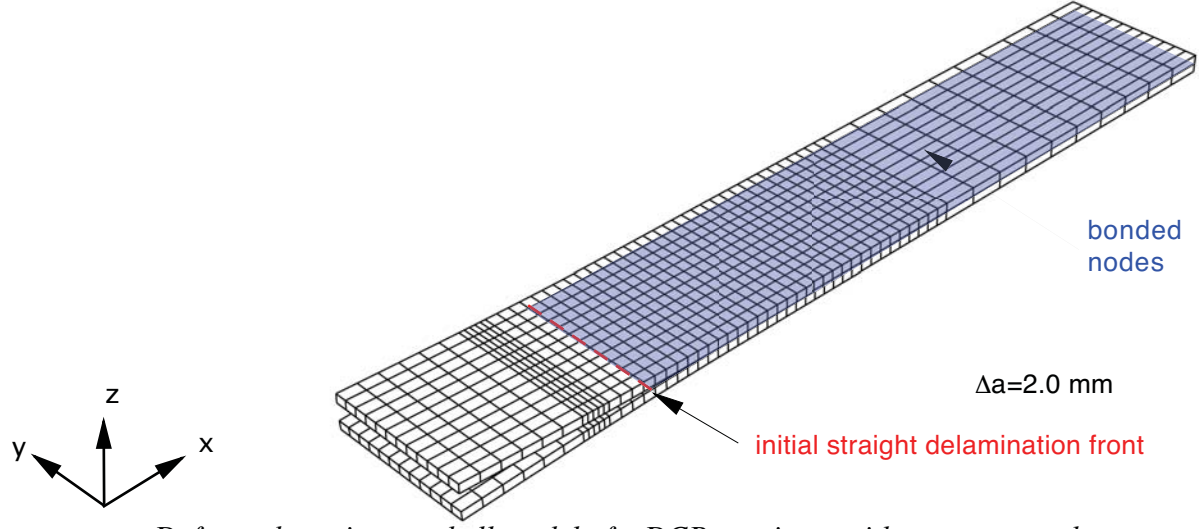
b. Deformed three-dimensional model of a DCB specimen with a coarse mesh
 Figure 16. Coarse full three-dimensional finite element models of a DCB specimen.



a. Deformed continuum-shell model of DCB specimen with a fine mesh



b. Deformed continuum-shell model of a DCB specimen with a coarse mesh



c. Deformed continuum-shell model of a DCB specimen with a coarse mesh

Figure 17. Continuum-shell finite element models of a DCB specimen.

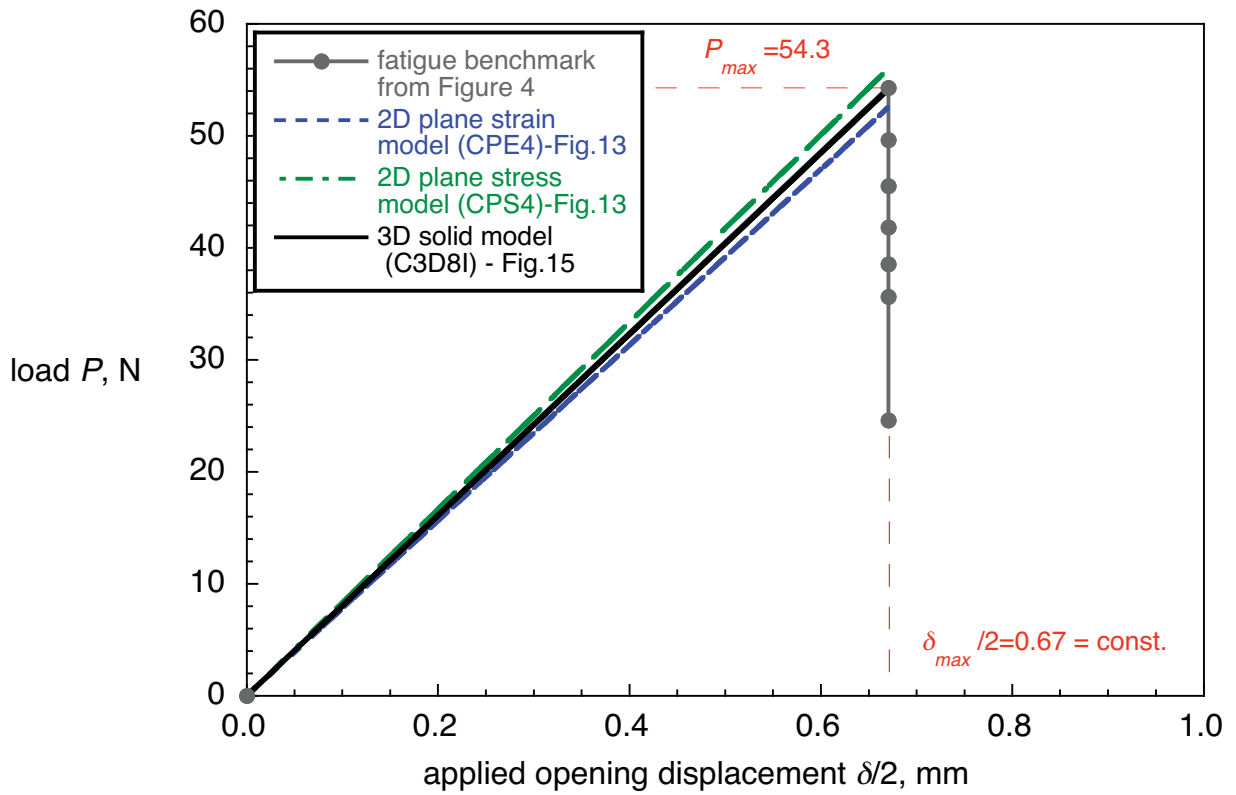


Figure 18. Critical load-displacement behavior for a DCB specimen.

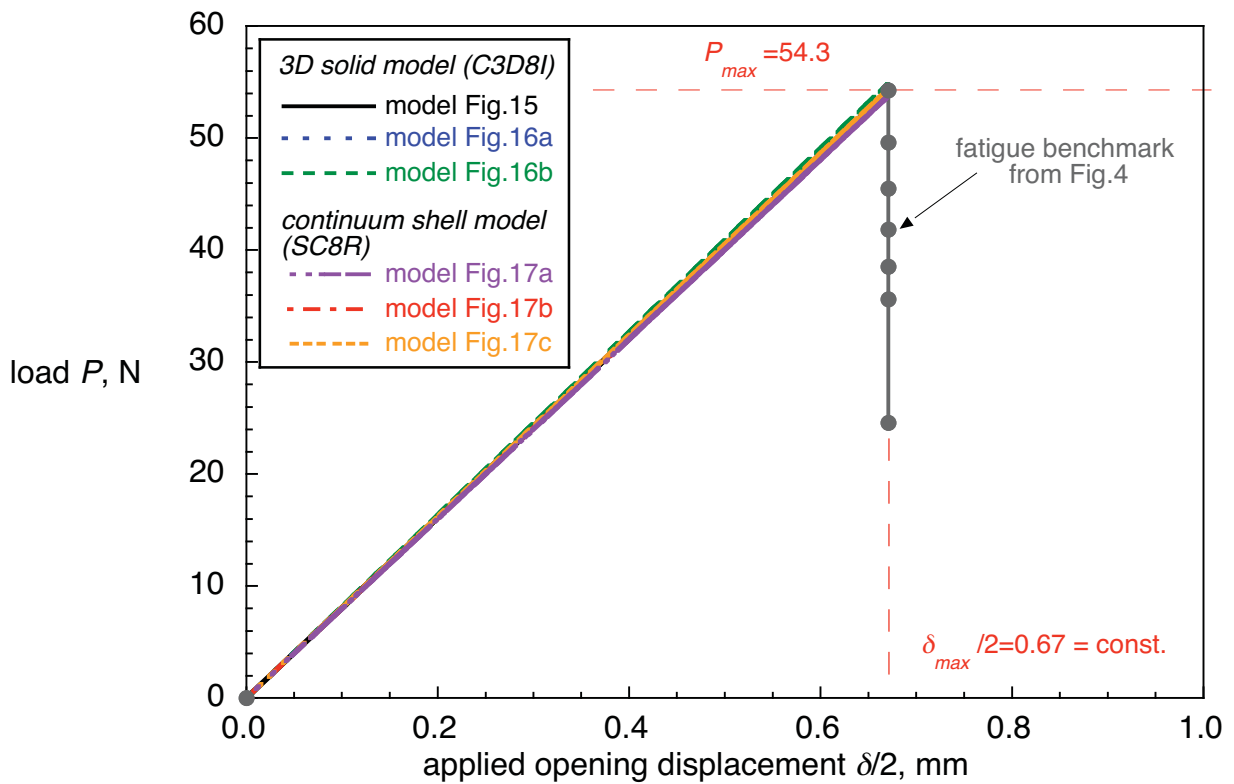


Figure 19. Critical load-displacement behavior for a DCB specimen.

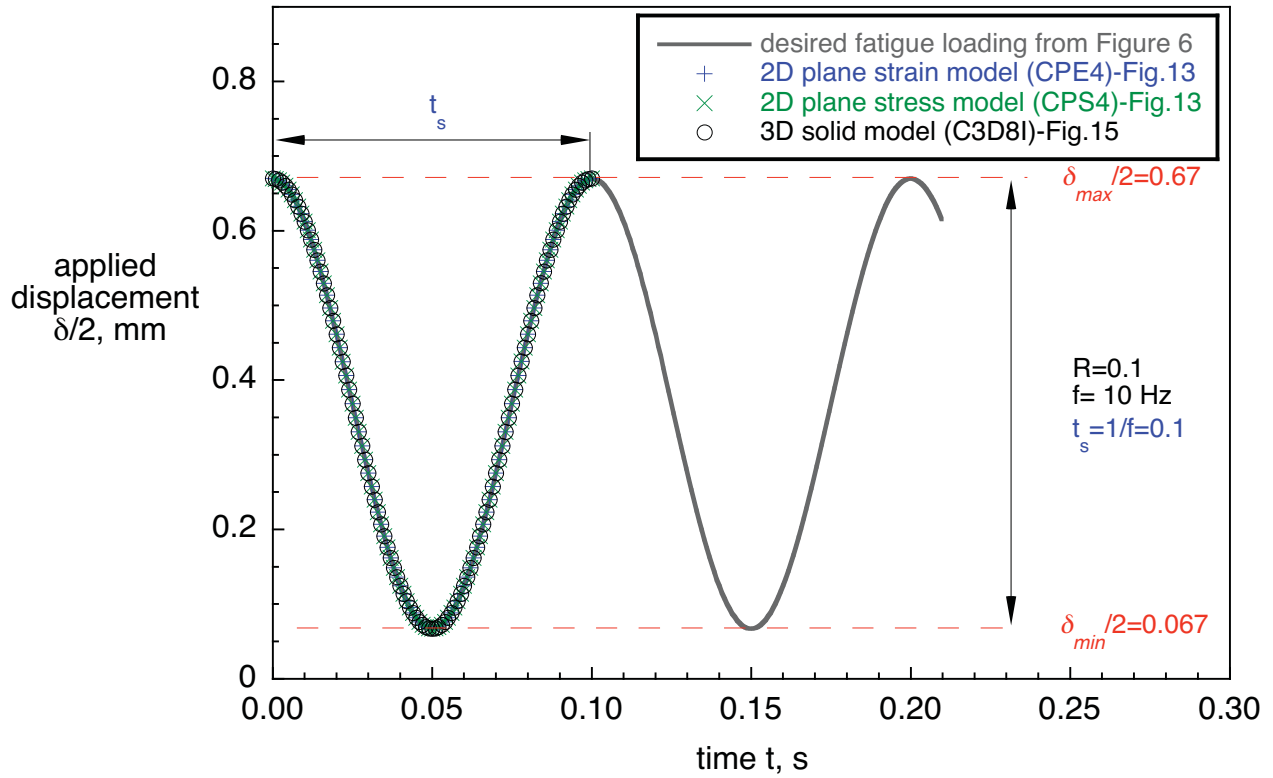


Figure 20. Cyclic fatigue loading for DCB specimen.

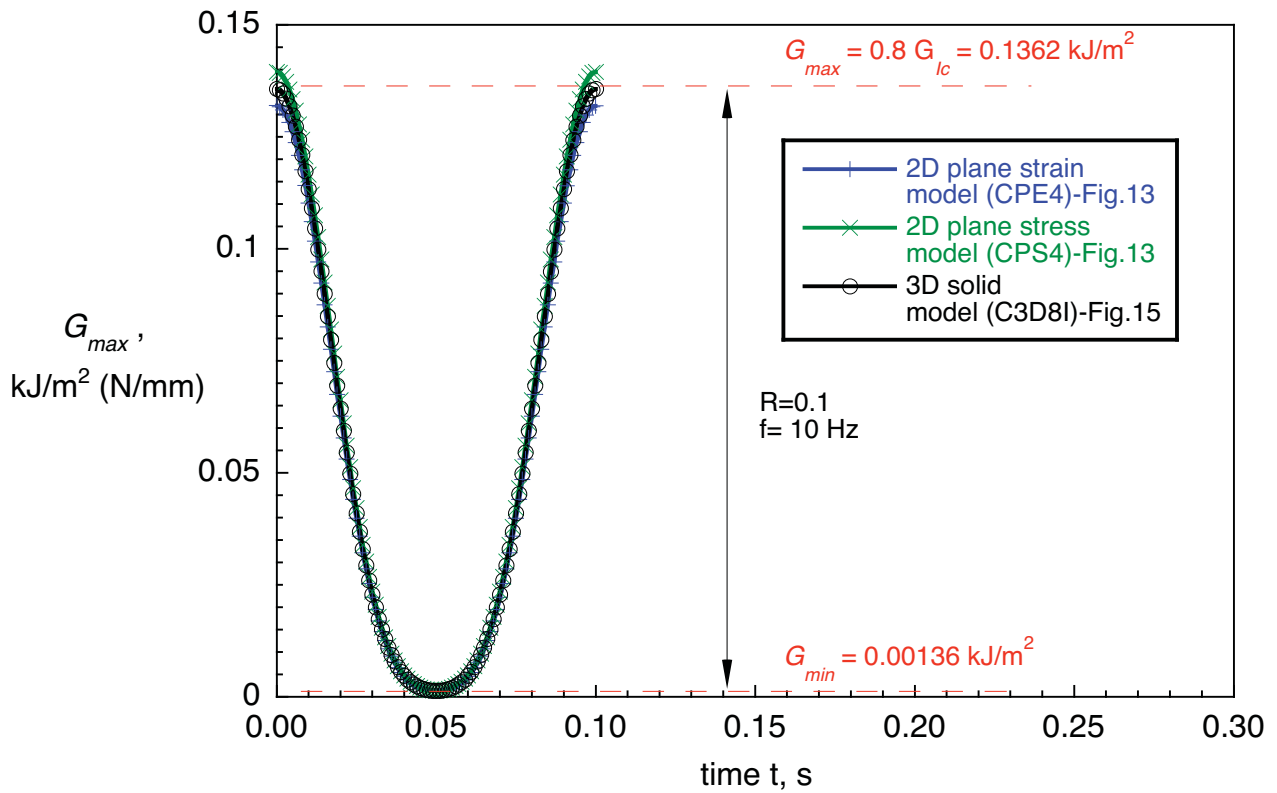


Figure 21. Computed energy release rate.

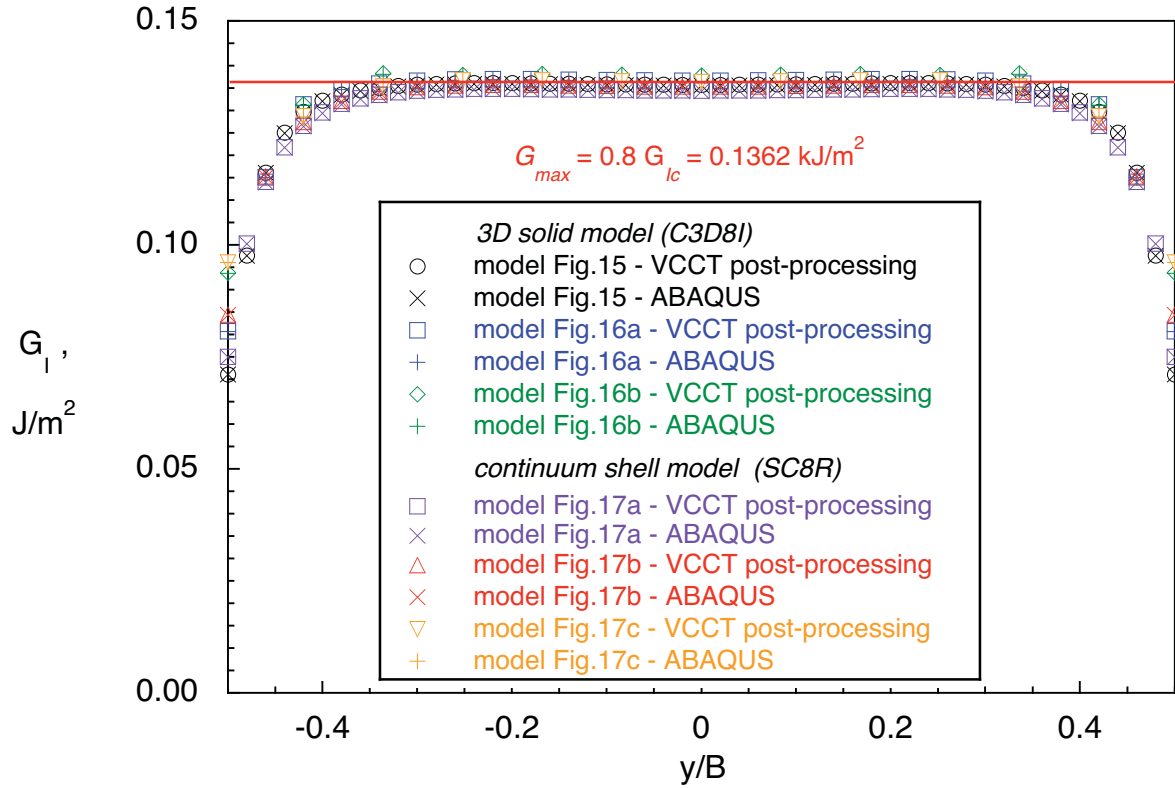


Figure 22. Computed strain energy release rate distribution across the width of a DCB specimen.

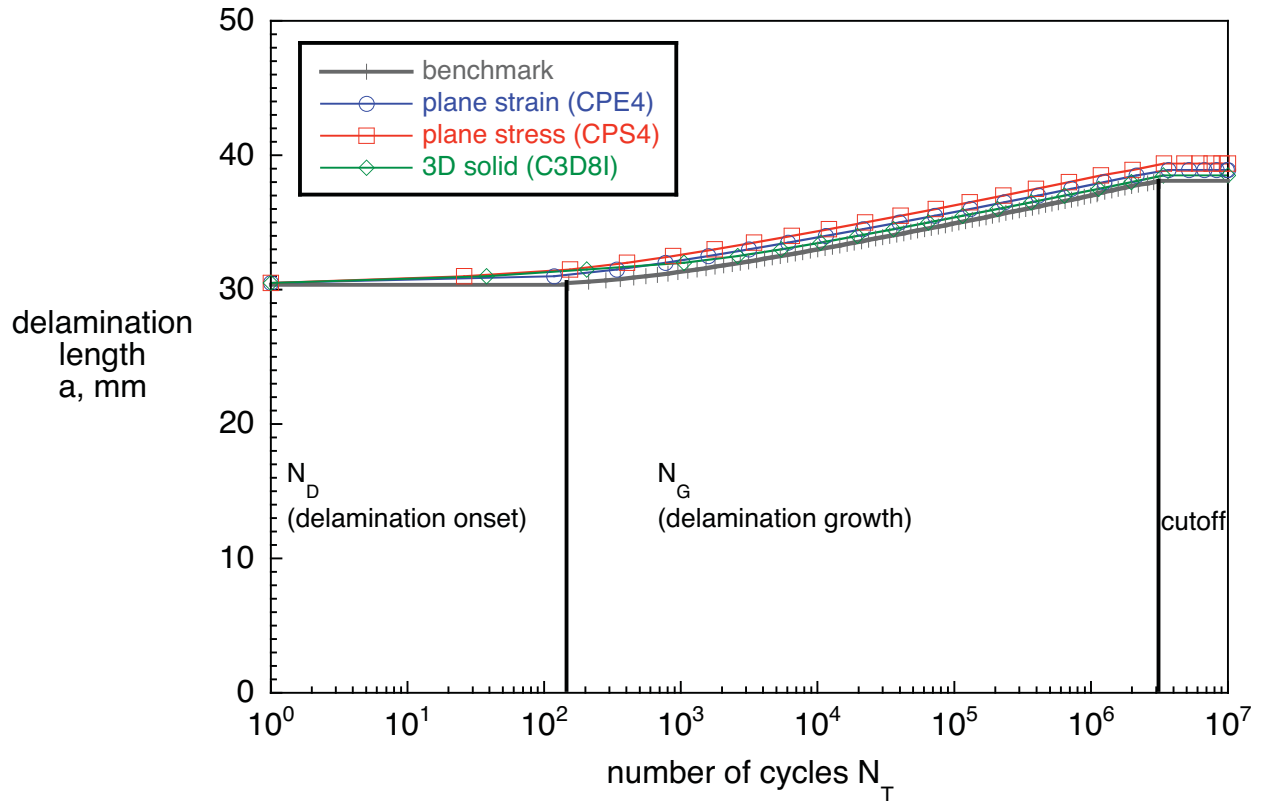


Figure 23. Computed delamination onset and growth: Initial results.

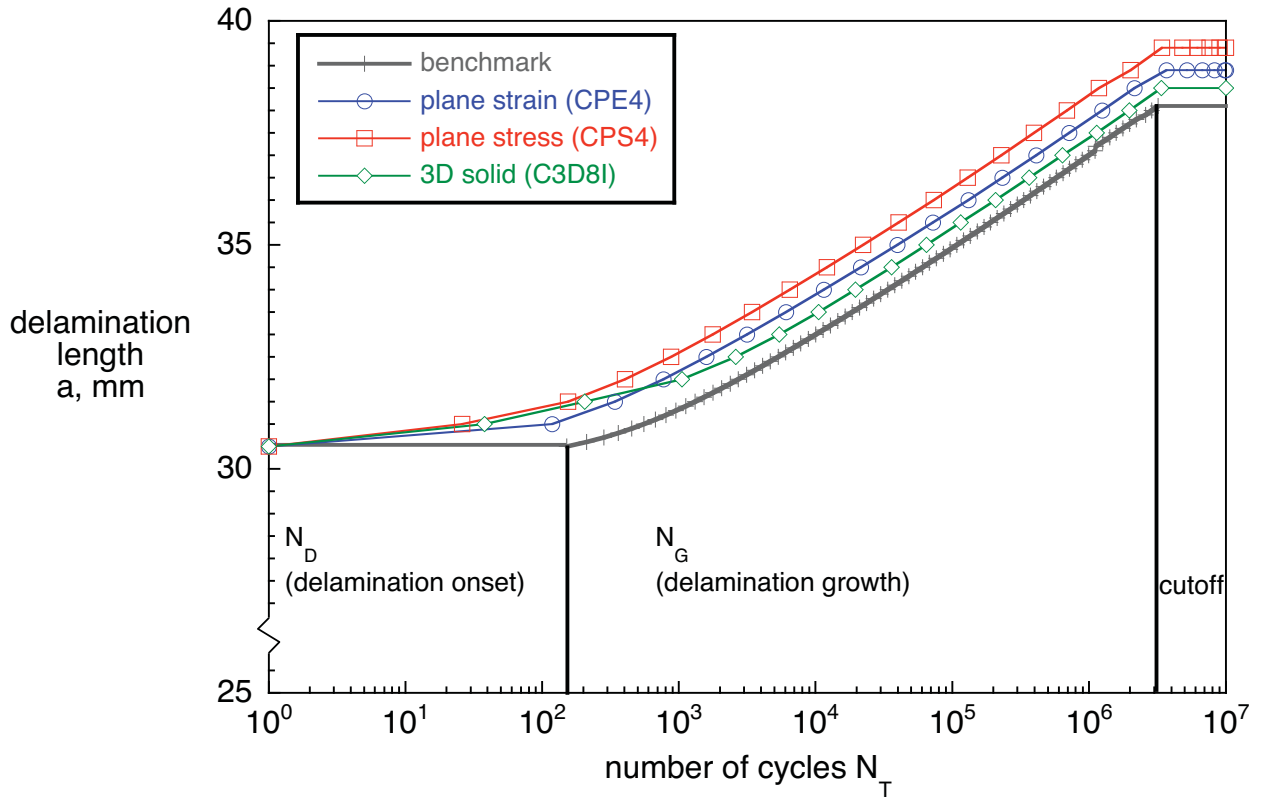


Figure 24. Computed delamination onset and growth: Detail of initial results.

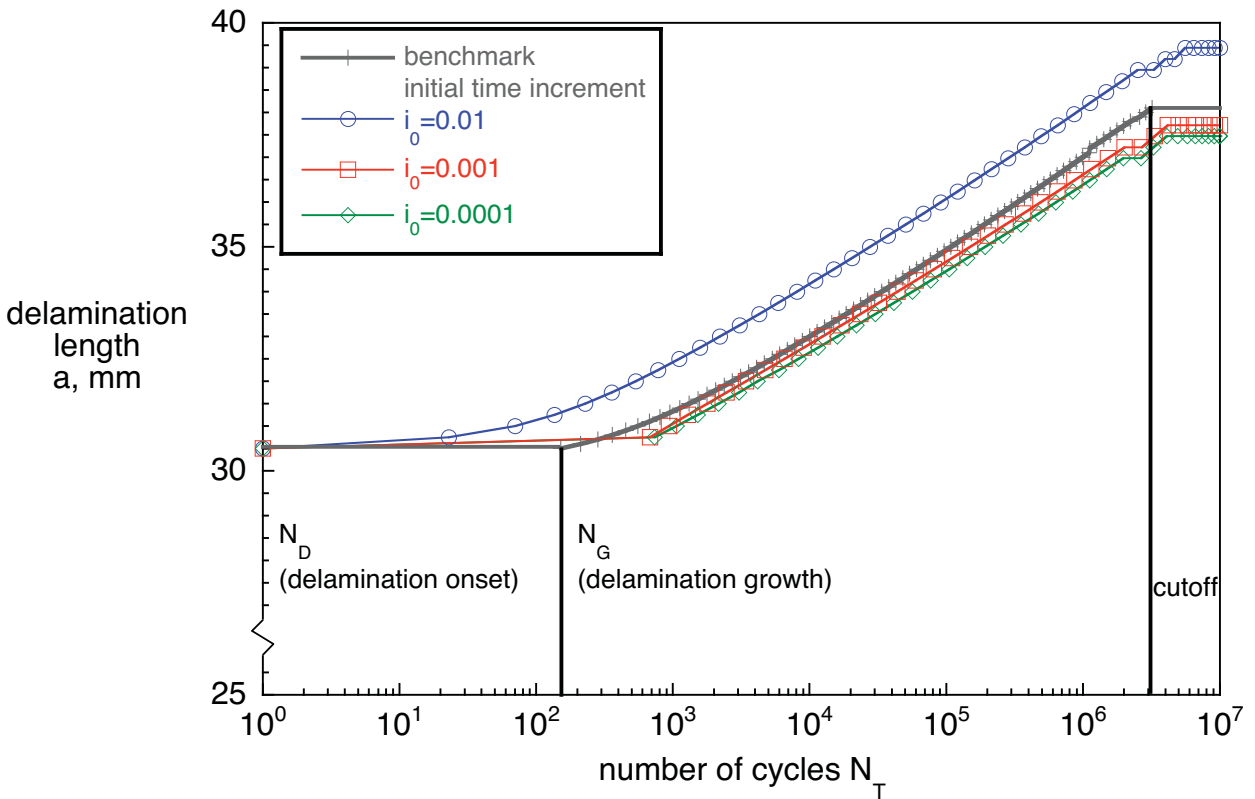


Figure 25. Computed delamination onset and growth obtained for different initial time increments.

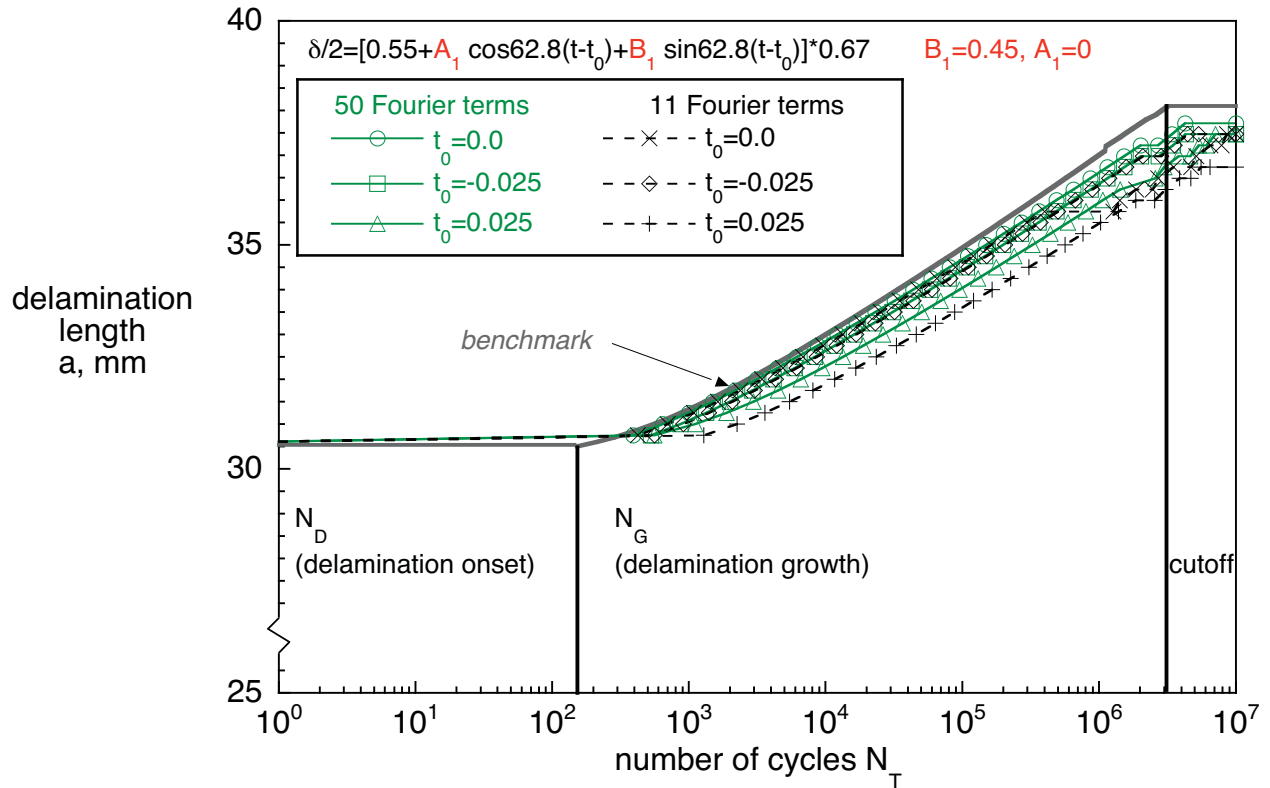


Figure 26. Computed delamination onset and growth obtained for sine representation of the cyclic loading.

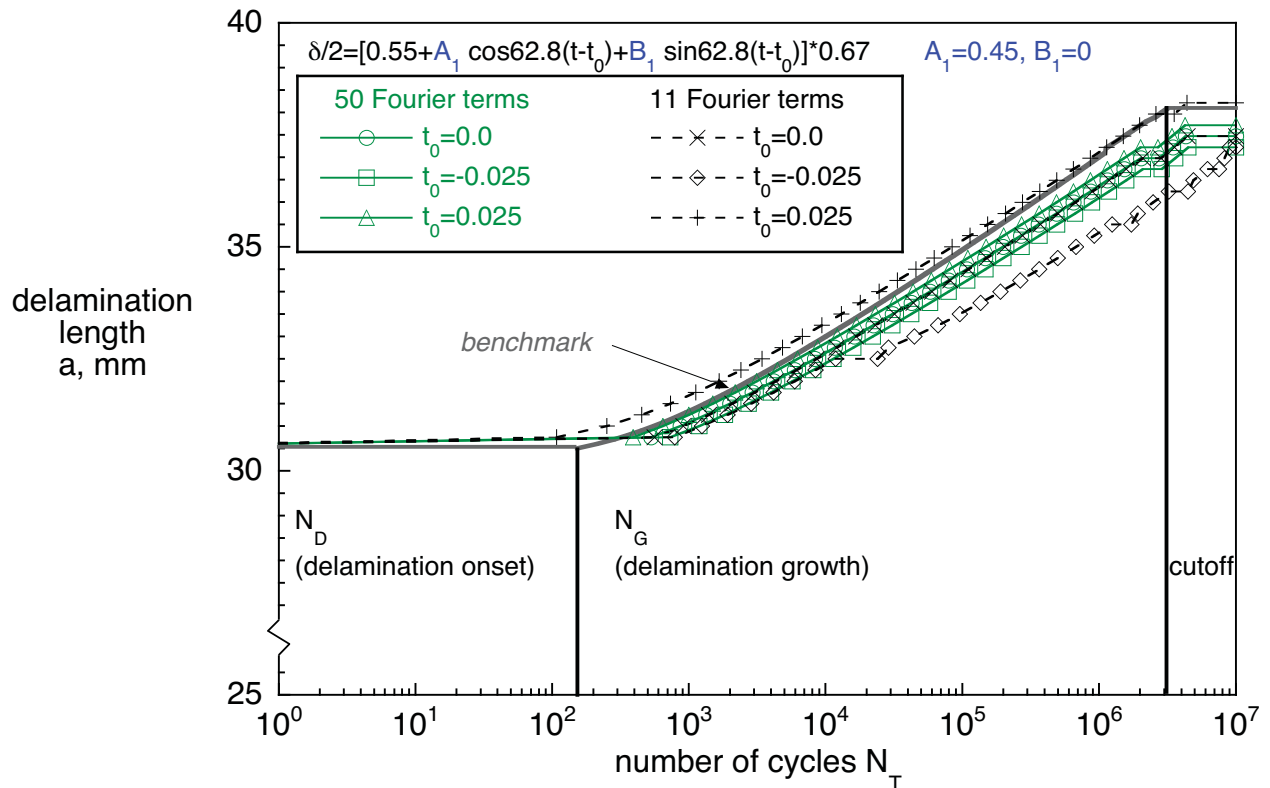


Figure 27. Computed delamination onset and growth obtained for cosine representation of the cyclic loading.

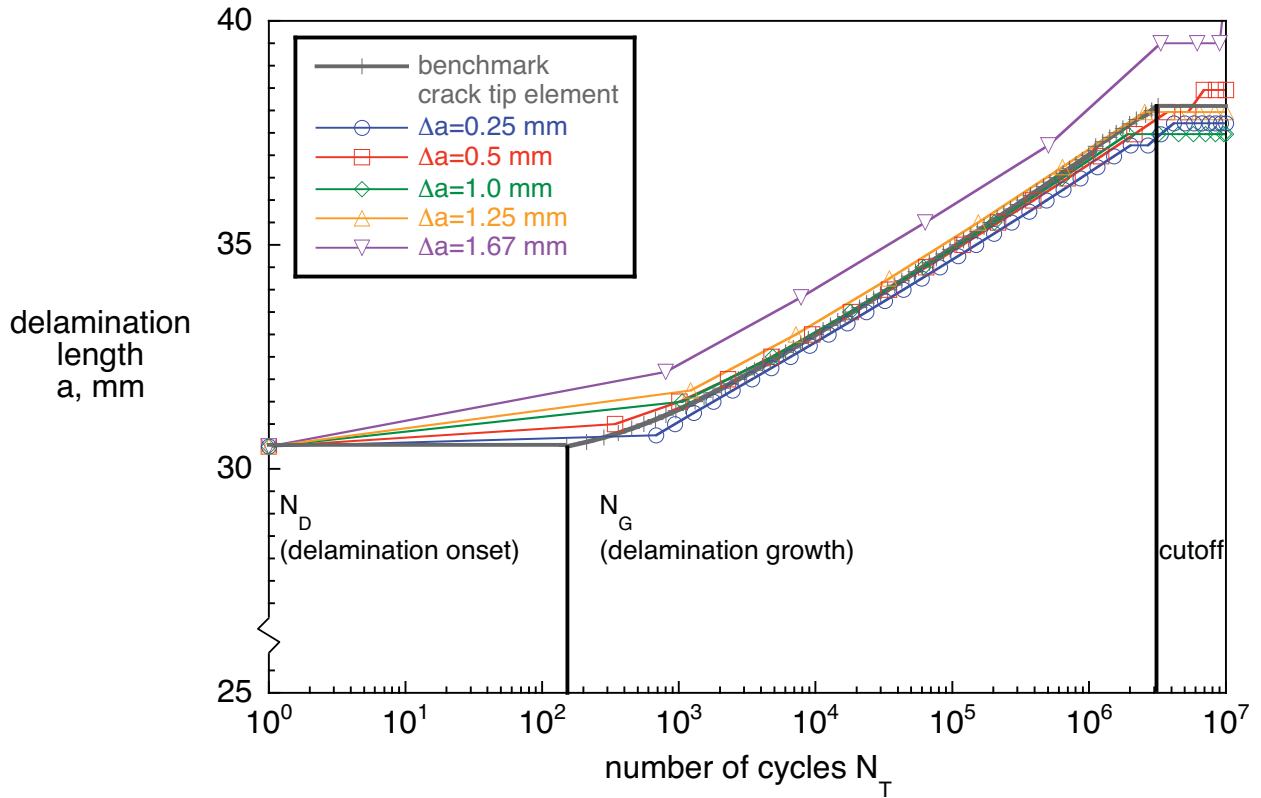


Figure 28. Computed delamination onset and growth behavior for different plane strain models.

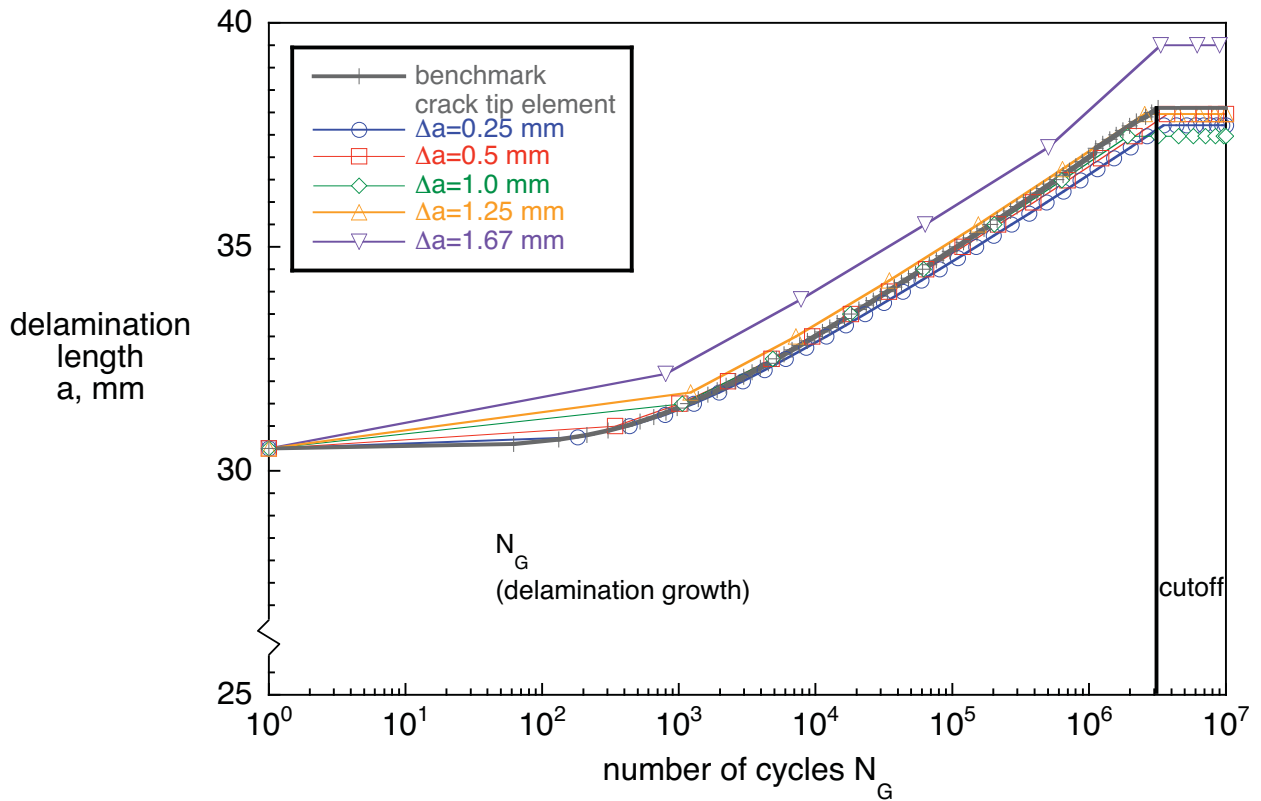


Figure 29. Computed stable delamination growth behavior for different plane strain models.

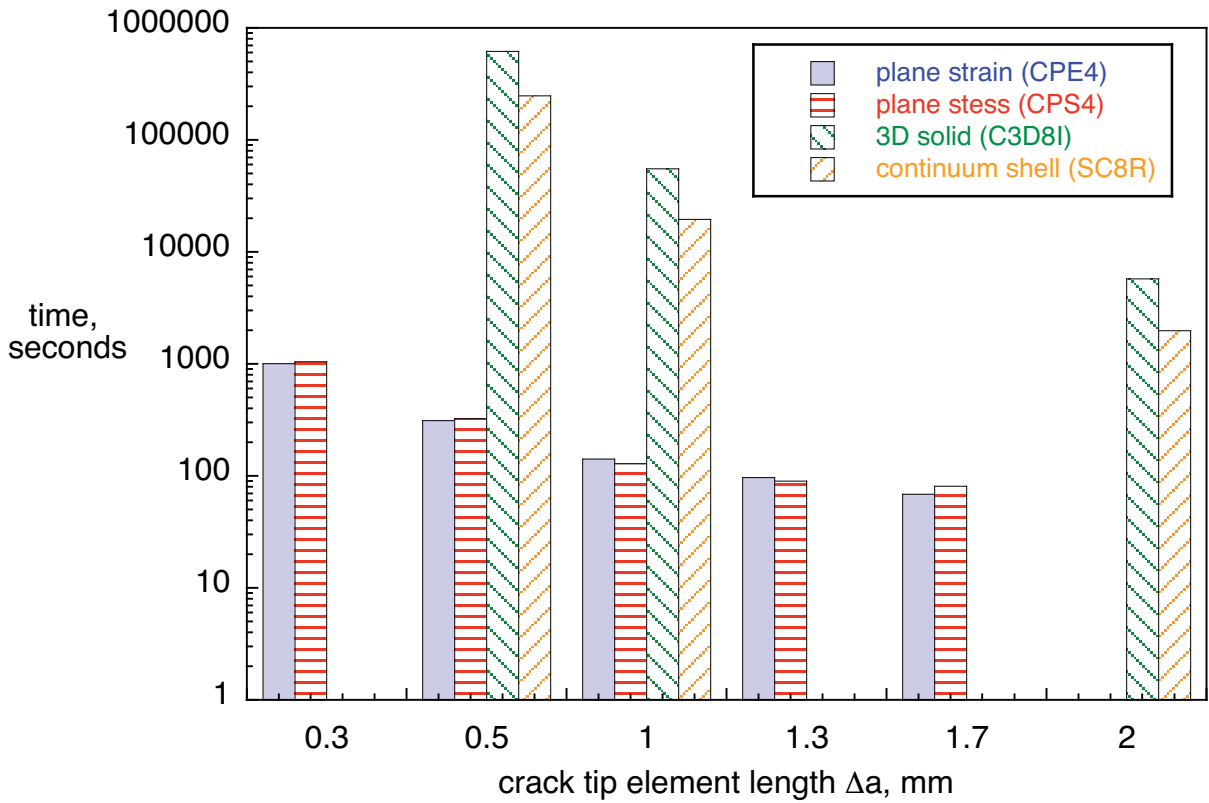


Figure 30. Required analysis time for models with different crack tip element lengths.

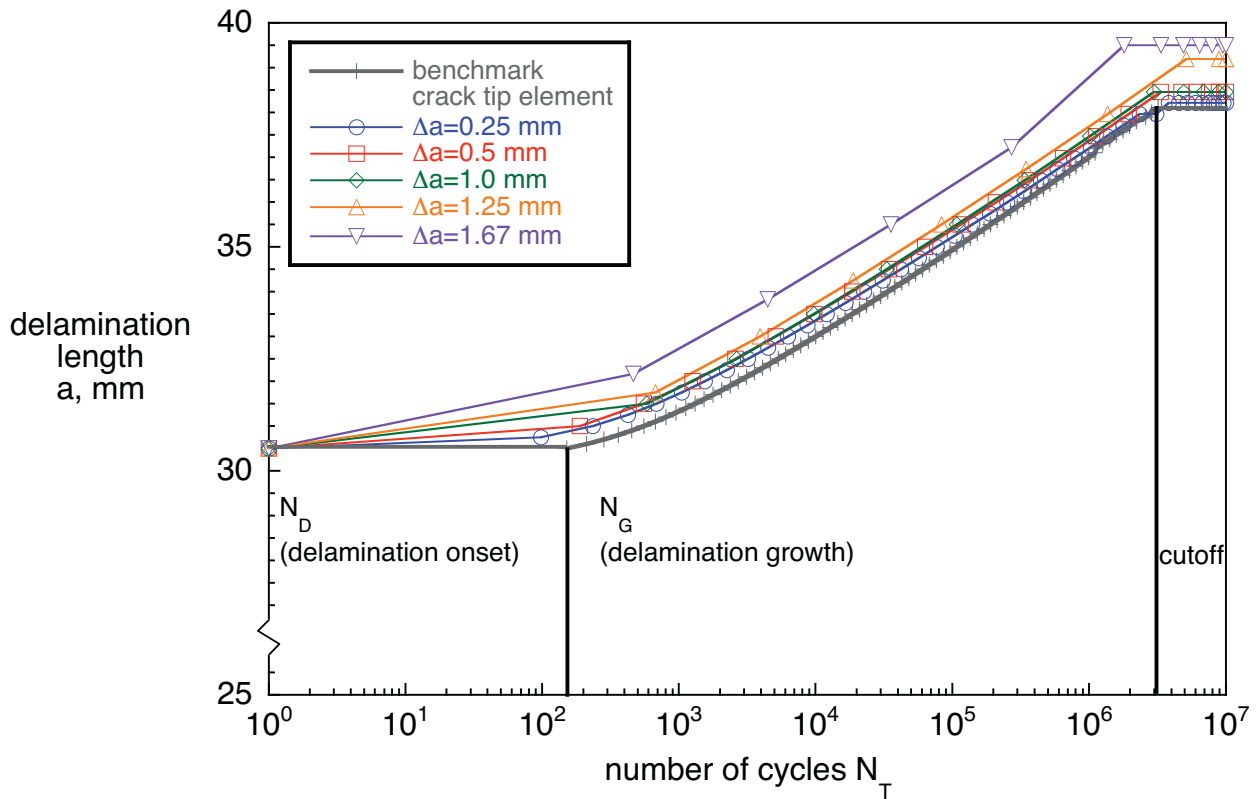


Figure 31. Computed delamination onset and growth behavior for different plane stress models.

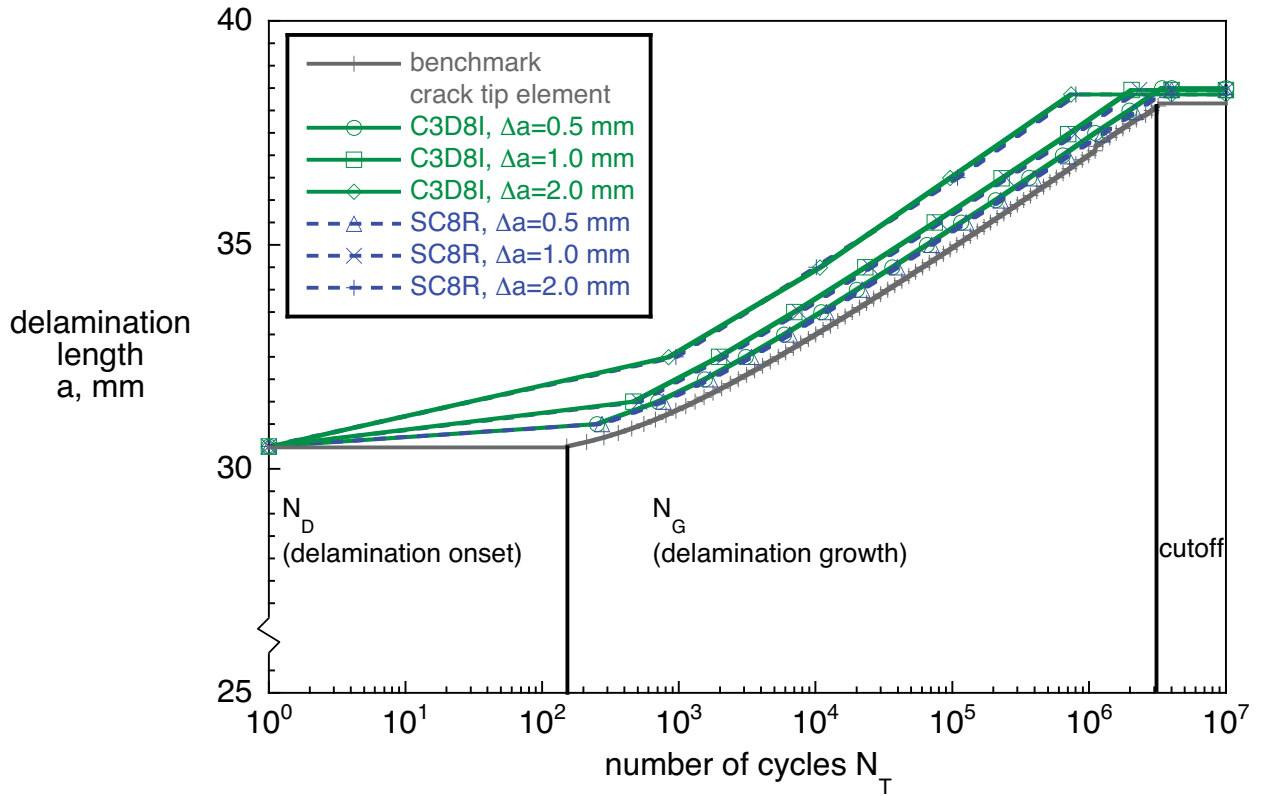


Figure 32. Computed delamination onset and growth behavior for different continuum models.

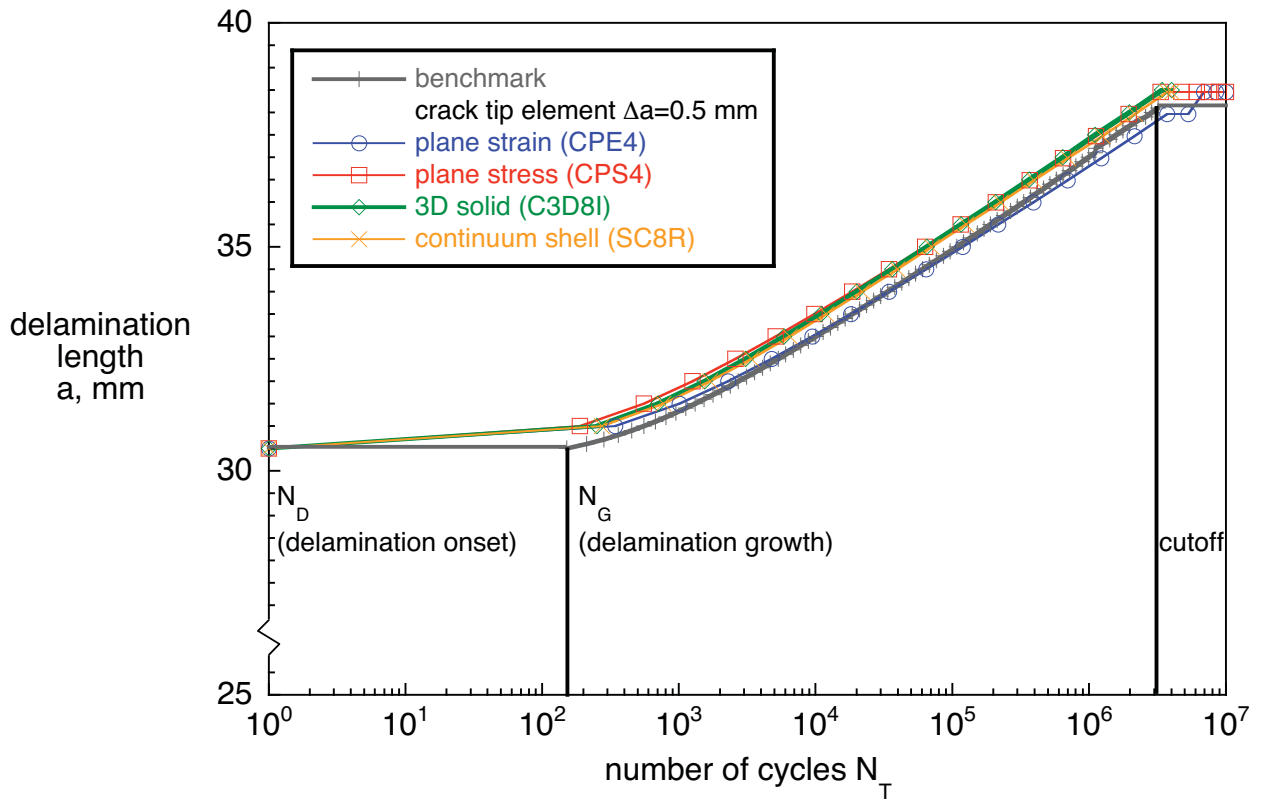


Figure 33. Computed delamination onset and growth behavior for different 2D and 3D models.

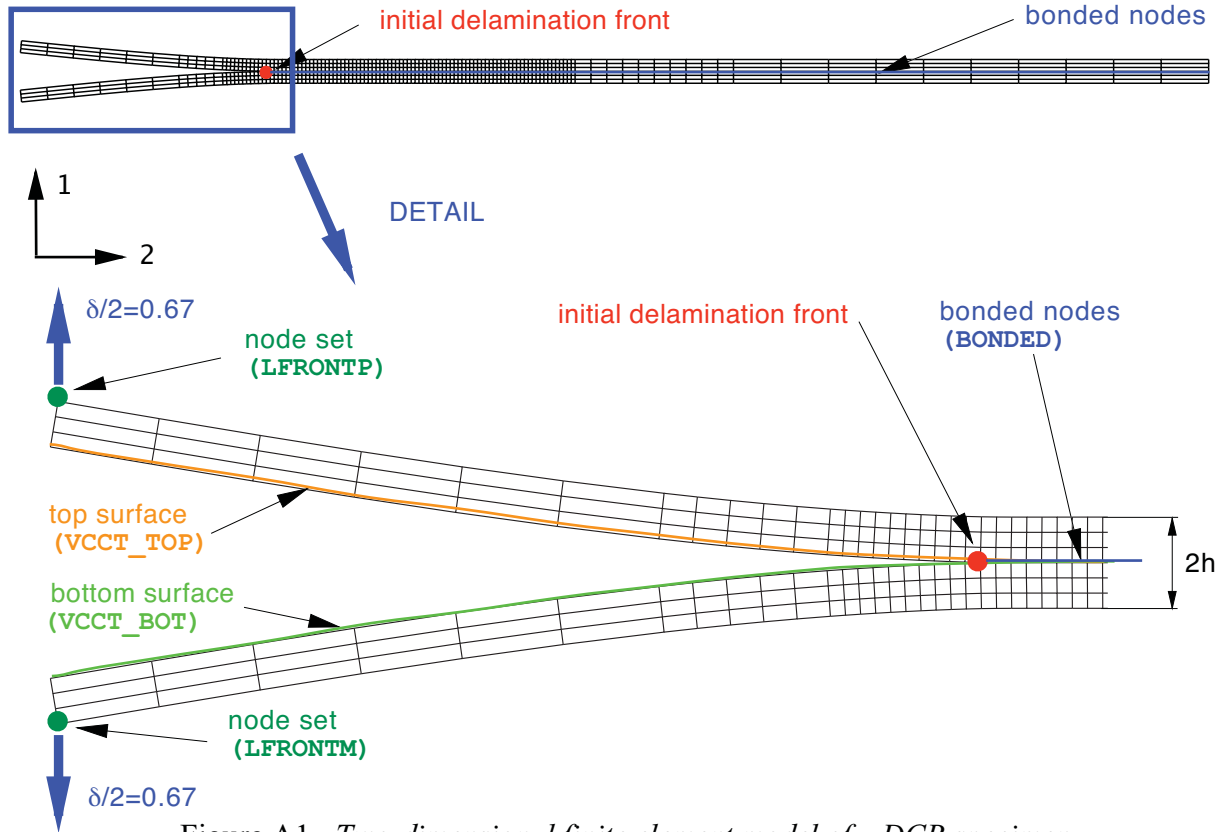


Figure A1. Two-dimensional finite element model of a DCB specimen.

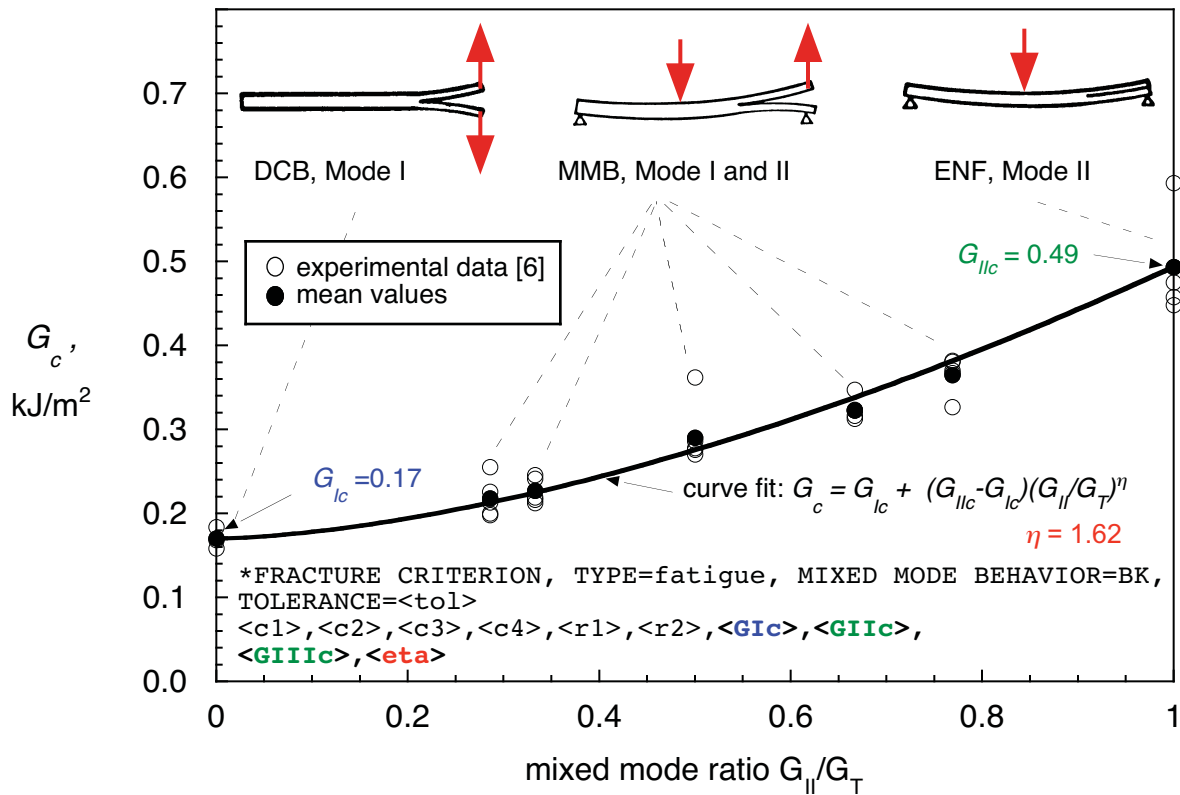


Figure A2. Mixed mode fracture criterion.

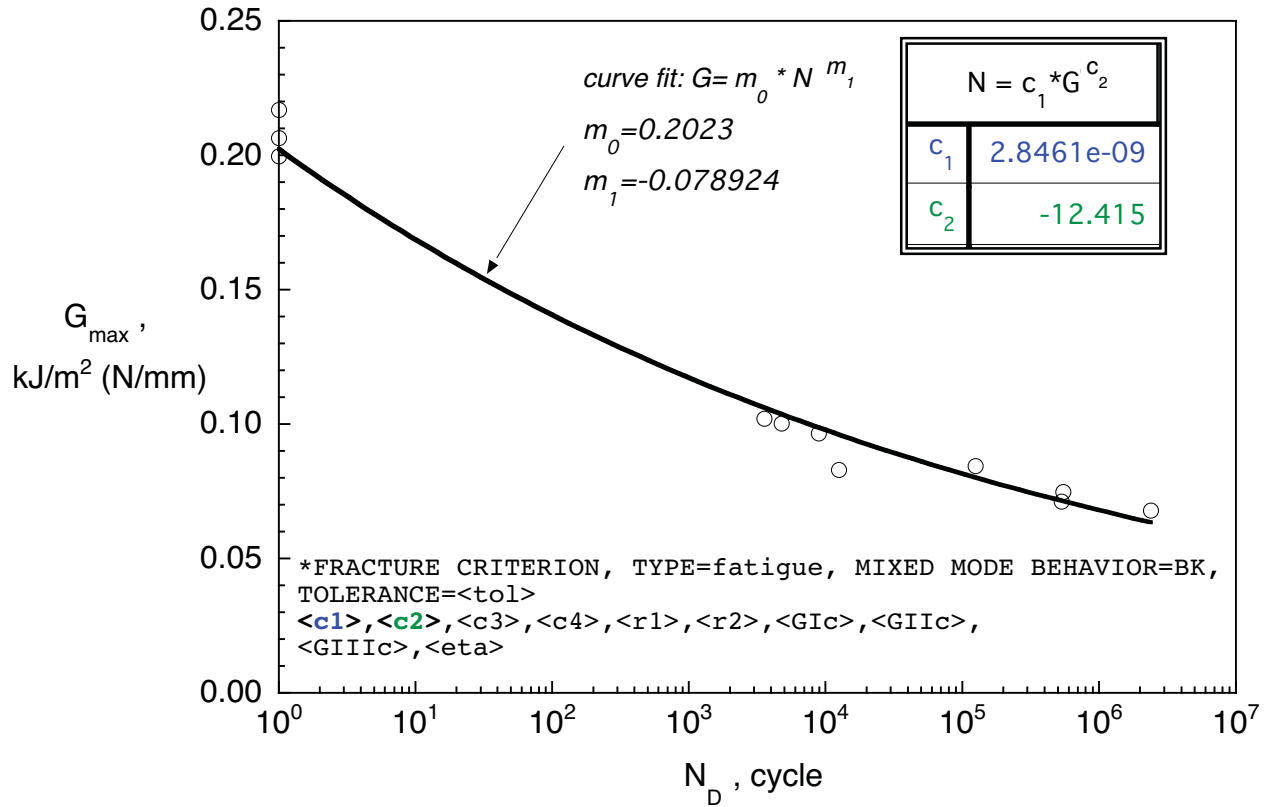


Figure A3. Delamination growth onset for DCB specimen.

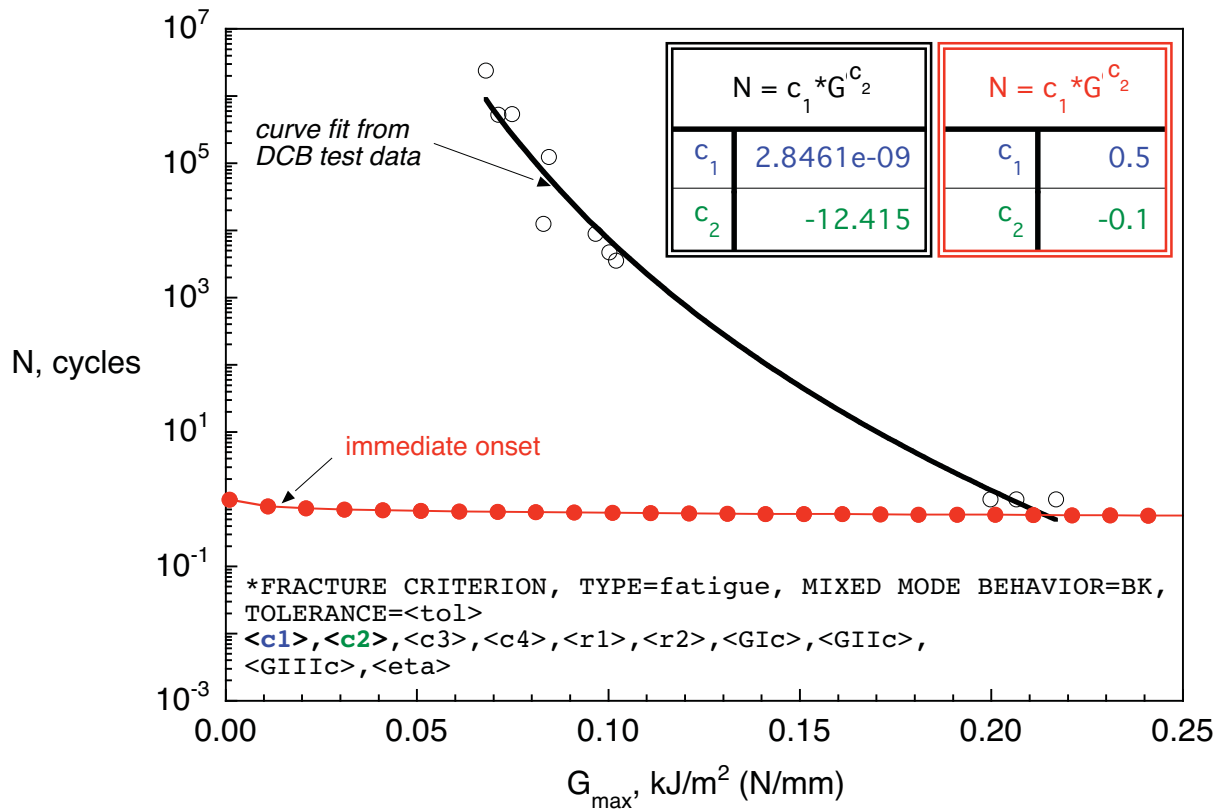


Figure A4. Delamination growth onset input data.

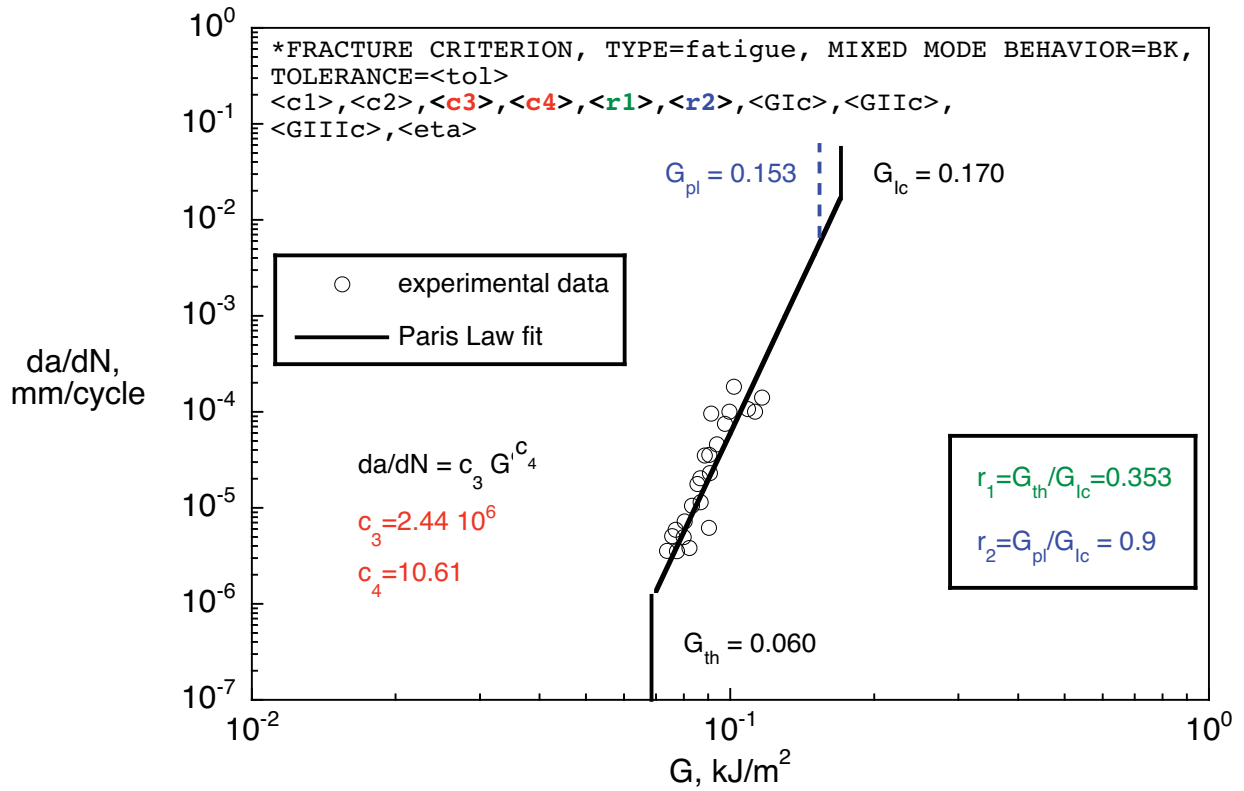


Figure A5. Delamination growth rate (Paris Law) for T300/914C.

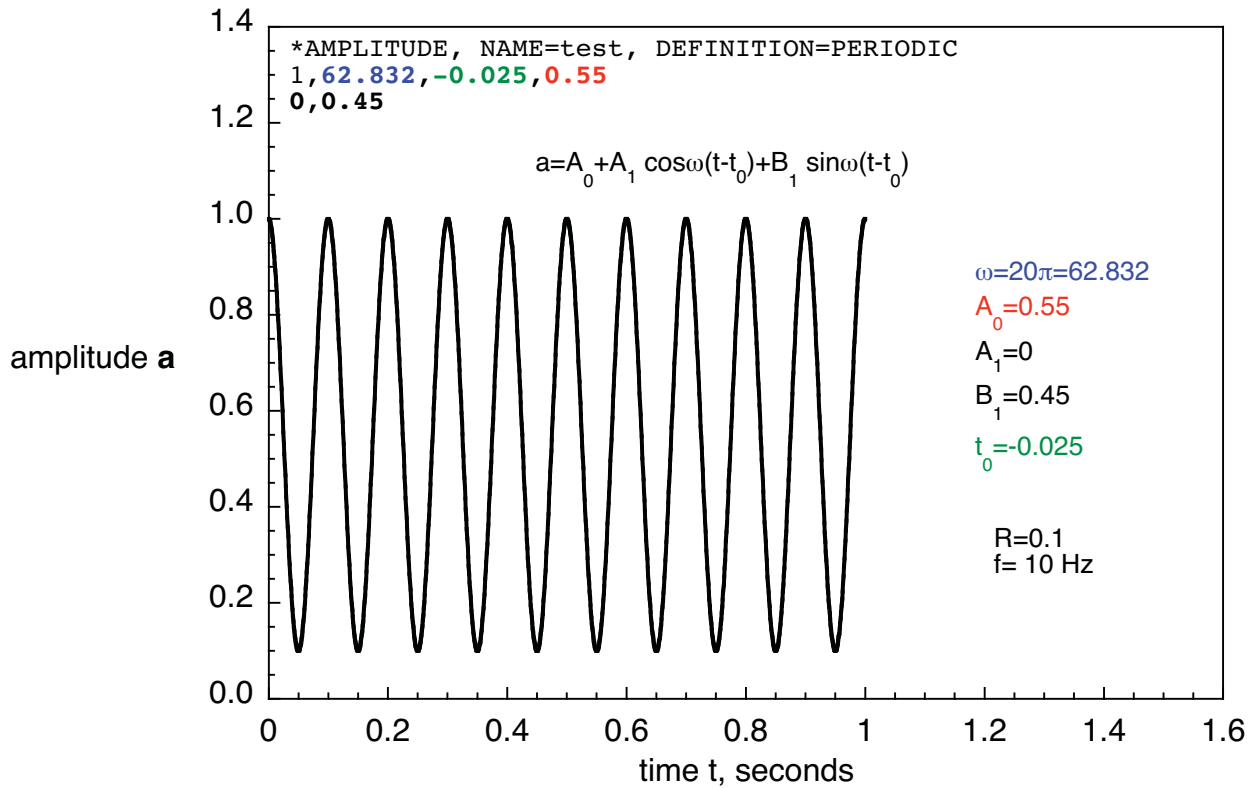


Figure A6. Amplitude curve (relative load magnitude).

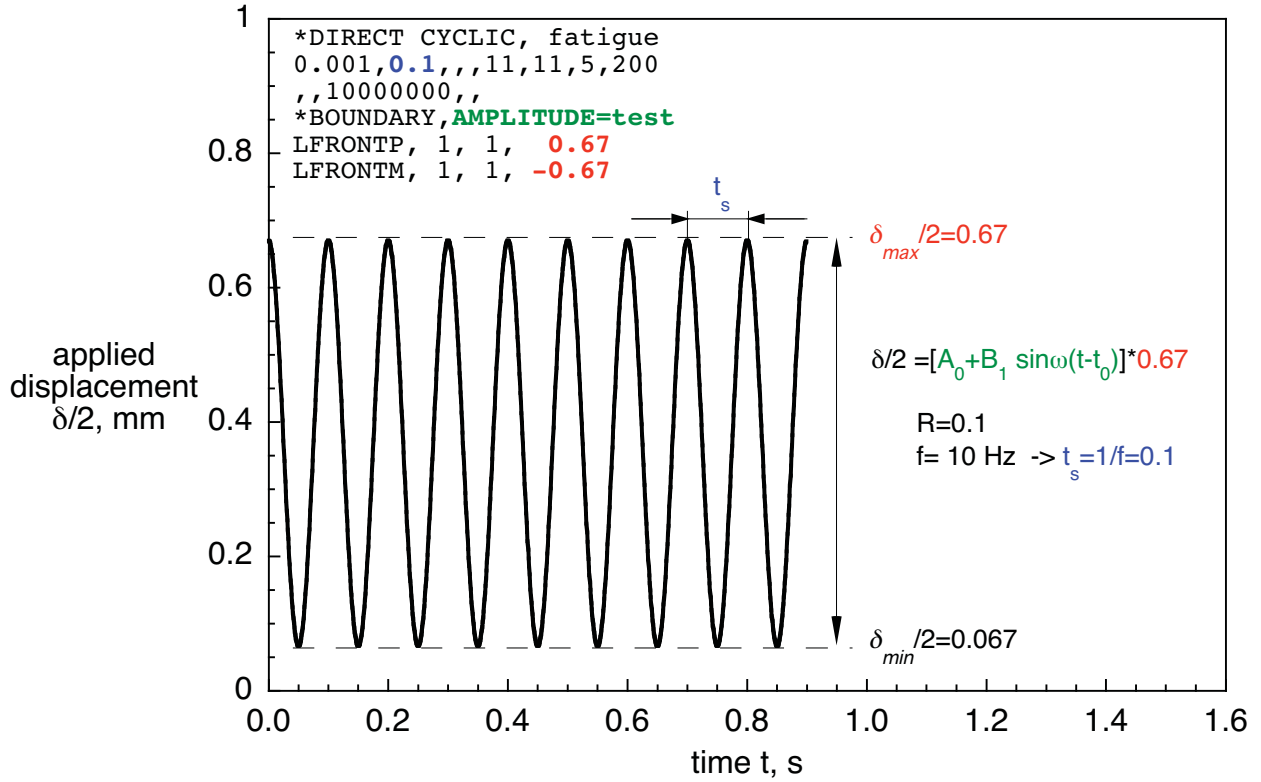


Figure A7. Cyclic fatigue loading input.

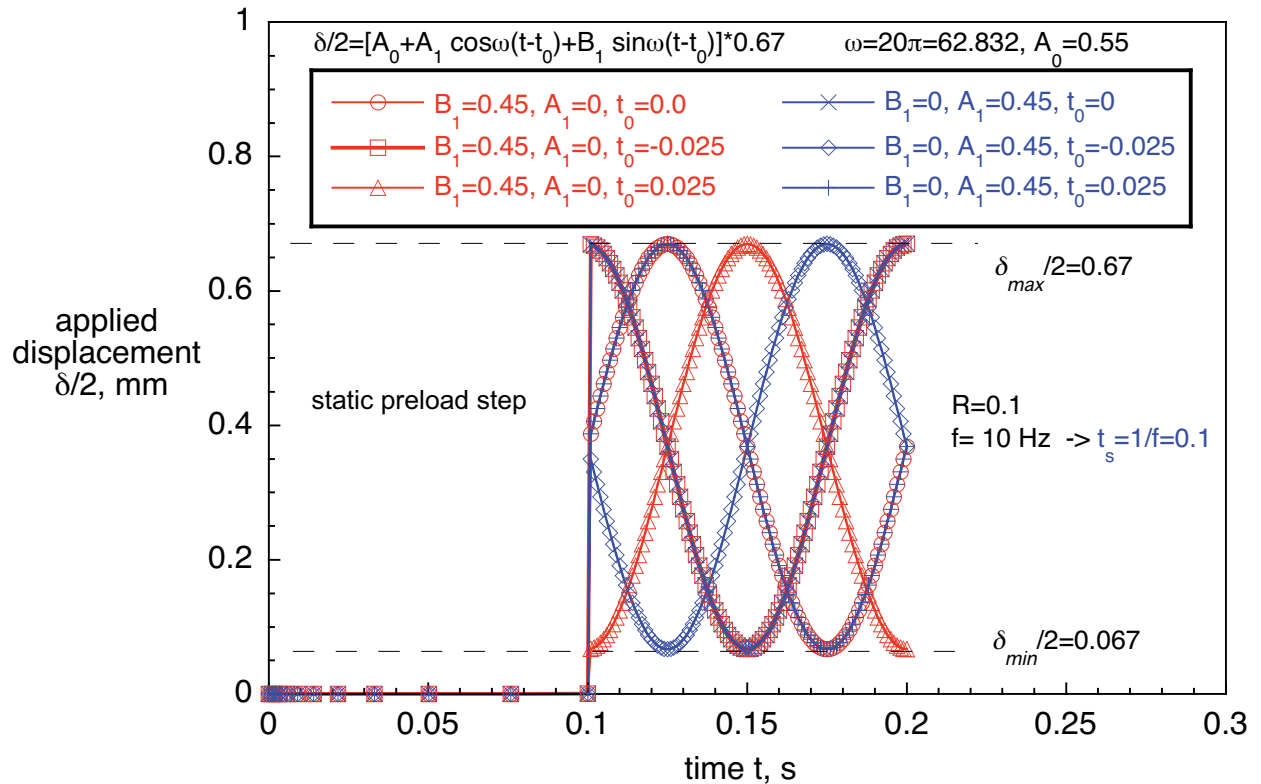


Figure A8. Cyclic fatigue loading for DCB specimen.

